MATHEMATICS OF COMPUTATION
Volume 00, Number 0, Pages 000–000
S 0025-5718(XX)0000-0

SEMIEXPLICIT SYMPLECTIC INTEGRATORS FOR NON-SEPARABLE HAMILTONIAN SYSTEMS

BUDDHIKA JAYAWARDANA AND TOMOKI OHSAWA

Abstract. We construct a symplectic integrator for non-separable Hamiltonian systems combining an extended phase space approach of Pihajoki and the symmetric projection method. The resulting method is semiexplicit in the sense that the main time evolution step is explicit whereas the symmetric projection step is implicit. The symmetric projection binds potentially diverging copies of solutions, thereby remedying the main drawback of the extended phase space approach. Moreover, our semiexplicit method is symplectic in the original phase space. This is in contrast to existing extended phase space integrators, which are symplectic only in the extended phase space. We demonstrate that our method exhibits an excellent long-time preservation of invariants, and also that it tends to be as fast as and can be faster than Tao's explicit modified extended phase space integrator particularly for small enough time steps and with higher-order implementations and for higher-dimensional problems.

1. Introduction

1.1. Non-Separable Hamiltonian Systems.

Consider a Hamiltonian system

$$\dot{q} = D_2 H(q,p), \qquad \dot{p} = -D_1 H(q,p). \tag{1}$$

with Hamiltonian $H\colon T^*\mathbb{R}^d \to \mathbb{R}$, where D_i stands for the partial derivative with respect to the i^{th} set of variables. Its underlying symplectic structure on the cotangent bundle $T^*\mathbb{R}^d$ is

$$\Omega := \mathbf{d}q \wedge \mathbf{d}p = \sum_{i=1}^{d} \mathbf{d}q^i \wedge \mathbf{d}p_i. \tag{2}$$

Throughout the paper, we shall use shorthands like above suppressing the summation symbol and indices when writing 2-forms.

The Hamiltonian H and the Hamiltonian system (1) are said to be *separable* if H can be written as $H(q,p) = K(p)+V(q)$ with some functions K and V, and *non-separable* otherwise. The separability is a crucial concept for the development of symplectic integrators for Hamiltonian systems because the separability sometimes turns implicit methods into explicit ones, and also makes the splitting method more amenable due to the fact that those flows of (1) with $H(q,p) = K(p)$ and $H(q,p) = V(q)$ are both exactly solvable; see, e.g., Sanz-Serna and Calvo [22], Leimkuhler and Reich [12], and Hairer et al. [11].

2020 *Mathematics Subject Classification.* 37M15,65P10.

Key words and phrases. Symplectic integrator, non-separable Hamiltonian, extended phase space.

On the other hand, developing an efficient symplectic integrator for non-separable Hamiltonian systems is a challenge. Although one can obtain explicit integrators for certain classes of non-separable Hamiltonian systems [1, 3, 17, 24, 26, 28–32], these methods are specialized for their respective specific forms of Hamiltonians, and do not seem to generalize to arbitrary non-separable Hamiltonians in a simple manner.

1.2. **Extended Phase Space Approach.** To our knowledge, the first explicit integrator for general non-separable Hamiltonian systems was developed by Pihajoki [21]. Specifically, in order to find an explicit integrator for non-separable Hamiltonian systems (1), Pihajoki proposed to solve the following extended system instead:

$$\begin{aligned} \dot{q} &= D_2 H(x,p), & \dot{p} &= -D_1 H(q,y), \\ \dot{x} &= D_2 H(q,y), & \dot{y} &= -D_1 H(x,p). \end{aligned} \tag{3}$$

One sees that if we impose the initial condition

$$(q(0), x(0), p(0), y(0)) = (q_0, q_0, p_0, p_0),$$

then the solution satisfies $(q(t), p(t)) = (x(t), y(t))$ for any $t \in \mathbb{R}$ (assuming that the solution exists and is unique), and $t \mapsto (q(t), p(t))$ coincides with the solution of the original system (1) with $(q(0), p(0)) = (q_0, p_0)$. In other words, the subspace

$$\mathcal{N} := \left\{ (q,q,p,p) \in T^*\mathbb{R}^{2d} \mid (q,p) \in T^*\mathbb{R}^d \right\} \subset T^*\mathbb{R}^{2d} \tag{4}$$

is an invariant submanifold of (3), and the system (3) restricted to this subspace gives two copies of the original system (1).

Notice also that (3) is a Hamiltonian system defined on the extended phase space

$$T^*\mathbb{R}^{2d} = \left\{ (q,x,p,y) \in \mathbb{R}^{4d} \mid (q,x) \in \mathbb{R}^{2d},\ (p,y) \in T^*_{(q,x)}\mathbb{R}^{2d} \cong \mathbb{R}^{2d} \right\}.$$

More specifically, the extended system (3) is a Hamiltonian system on $T^*\mathbb{R}^{2d}$ with the extended Hamiltonian

$$\hat{H} \colon T^*\mathbb{R}^{2d} \to \mathbb{R}; \qquad \hat{H}(q,x,p,y) := H(q,y) + H(x,p)$$

and the following standard symplectic form on $T^*\mathbb{R}^{2d}$:

$$\hat{\Omega} := \mathbf{d}q \wedge \mathbf{d}p + \mathbf{d}x \wedge \mathbf{d}y. \tag{5}$$

Let us give a more geometric and intuitive interpretation; see also Figure 1. Let $\hat{X}$ be the vector field on $T^*\mathbb{R}^{2d}$ for the extended system (3):

$$\hat{X}(q,x,p,y) := (D_2 H(x,p),\ D_2 H(q,y),\ -D_1 H(q,y),\ -D_1 H(x,p)).$$

If we restrict $\hat{X}$ to the subspace $\mathcal{N}$, then $\hat{X}(q,q,p,p)$ consists of two copies of the Hamiltonian vector field

$$X(q,p) := (D_2 H(q,p),\ -D_1 H(q,p))$$

on the original phase space $T^*\mathbb{R}^d$. Therefore, the dynamics in $\mathcal{N}$ defined by $\hat{X}$ is two copies of the Hamiltonian dynamics defined by X on $T^*\mathbb{R}^d$. Hence they are essentially the same dynamics.

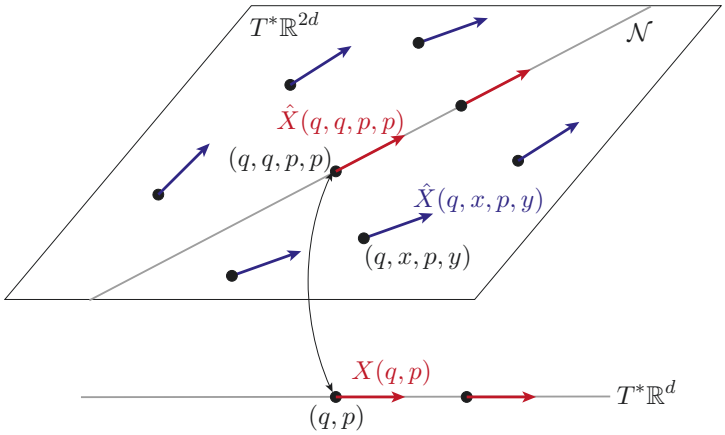

FIGURE 1. Hamiltonian vector field $\hat{X}$ on extended phase space $T^*\mathbb{R}^{2d}$ restricted to $\mathcal{N}$ gives two copies of Hamiltonian vector field X on $T^*\mathbb{R}^d$.

1.3. **Extended Phase Space Integrators.** The salient feature of the above approach by Pihajoki [21] is that the Hamiltonian is now separable: Defining

$$\hat{H}_A(q,x,p,y) := H(q,y), \qquad \hat{H}_B(q,x,p,y) := H(x,p),$$

we have

$$\hat{H}(q,x,p,y) = \hat{H}_A(q,x,p,y) + \hat{H}_B(q,x,p,y) = H(q,y) + H(x,p).$$

Furthermore, the flows $\hat{\Phi}_t^A, \hat{\Phi}_t^B \colon T^*\mathbb{R}^{2d} \to T^*\mathbb{R}^{2d}$ corresponding to the Hamiltonians $\hat{H}_A$ and $\hat{H}_B$ are exactly solvable for any $t \in \mathbb{R}$. Indeed, with $\hat{H}_A$, we have

$$\begin{aligned} \dot{q} &= 0, & \dot{p} &= -D_1 H(q,y), \\ \dot{x} &= D_2 H(q,y), & \dot{y} &= 0. \end{aligned}$$

and so

$$\hat{\Phi}_t^A(q_0,x_0,p_0,y_0) = (q_0,\, x_0 + t\, D_2 H(q_0,y_0),\, p_0 - t\, D_1 H(q_0,y_0),\, y_0),$$

whereas, with $\hat{H}_B$, we have

$$\begin{aligned} \dot{q} &= D_2 H(x,p), & \dot{p} &= 0, \\ \dot{x} &= 0, & \dot{y} &= -D_1 H(x,p). \end{aligned}$$

and so

$$\hat{\Phi}_t^B(q_0,x_0,p_0,y_0) = (q_0 + t\, D_2 H(x_0,p_0),\, x_0,\, p_0,\, y_0 - t\, D_1 H(x_0,p_0)).$$

One can therefore construct a 2^{nd}-order explicit integrator by using the Strang splitting [23]:

$$\hat{\Phi}_{\Delta t} := \hat{\Phi}_{\Delta t/2}^A \circ \hat{\Phi}_{\Delta t}^B \circ \hat{\Phi}_{\Delta t/2}^A \colon T^*\mathbb{R}^{2d} \to T^*\mathbb{R}^{2d} \tag{6}$$

with time step Δt.

1.4. **Issues of Extended Phase Space Integrators.** As ingenious as the above idea is, there are some issues to be addressed for such extended phase space integrators.

Perhaps the most significant issue is that the defect $(x-q, y-p)$ in the phase space copies (q,p) and (x,y) tends to grow in time numerically. This can be detrimental in the long run because the solution of the extended system (3) may diverge from that of the original system (1) when $(x,y) \neq (q,p)$. We shall demonstrate it in Figure 4 in Section 4.4 below.

As a remedy for this drawback, Tao [27] suggested to solve an alternative extended system

$$\begin{aligned} \dot{q} &= D_2 H(x,p) + \omega(p-y), & \dot{p} &= -D_1 H(q,y) - \omega(q-x), \\ \dot{x} &= D_2 H(q,y) + \omega(y-p), & \dot{y} &= -D_1 H(x,p) - \omega(x-q) \end{aligned} \tag{7}$$

with some $\omega \in \mathbb{R}$. Note that the above system (7) is also a Hamiltonian system on the extended phase space $T^*\mathbb{R}^{2d}$ with the Hamiltonian

$$\hat{H}_A(q,x,p,y) + \hat{H}_B(q,x,p,y) + \hat{H}_C(q,x,p,y),$$

where

$$\hat{H}_C(q,x,p,y) := \frac{\omega}{2}\big((x-q)^2 + (y-p)^2\big).$$

Also, the subspace $\mathcal{N} \subset T^*\mathbb{R}^{2d}$ (defined in (4)) is again an invariant manifold of (7) as well.

The flow corresponding to $\hat{H}_C$ is also exactly solvable, and so one can construct symplectic integrators using splitting methods based on the three flows corresponding to the three Hamiltonians. For example, Tao [27] constructed the following 2^{nd}-order integrator:

$$\hat{\Phi}^A_{\Delta t/2} \circ \hat{\Phi}^B_{\Delta t/2} \circ \hat{\Phi}^C_{\Delta t} \circ \hat{\Phi}^B_{\Delta t/2} \circ \hat{\Phi}^A_{\Delta t/2} \colon T^*\mathbb{R}^{2d} \to T^*\mathbb{R}^{2d}. \tag{8}$$

It is demonstrated numerically in [27] (see also Figure 4 in Section 4.4 below) that the insertion of the C-step effectively suppresses the growth of the defect $(x-q, y-p)$. We note however that the defect is far from negligible as we shall address later.

We also mention in passing that various modifications of extended phase space integrators are proposed, especially for relativistic dynamics with astrophysical applications [13–15, 20, 34].

Another issue is that, while these integrators are symplectic in the extended phase space $T^*\mathbb{R}^{2d}$, it is not clear how that is related to the symplecticity of the original system (1) in $T^*\mathbb{R}^d$. More specifically, given a discrete flow $\{(q_n, x_n, p_n, y_n)\}_{n\geq 0}$ on $T^*\mathbb{R}^{2d}$ constructed by one of the above extended phase space integrators, one easily sees that the extended symplectic form $\hat{\Omega}$ defined in (5) is preserved, but it is not clear if the projected dynamics $\{(q_n, p_n)\}_{n\geq 0}$ on $T^*\mathbb{R}^d$ preserves the symplectic form Ω defined in (2). In fact, such a projected dynamics on $T^*\mathbb{R}^d$ is not well-defined because the time evolution $(q_n, p_n) \mapsto (q_{n+1}, p_{n+1})$ depends on (x_n, y_n) as well.

1.5. **Main Result and Outline.** We propose to combine the above extended phase space approach of Pihajoki [21] with the symmetric projection method (see, e.g., [11, Section V.4.1]) to construct a symplectic integrator for non-separable Hamiltonian systems (1).

The resulting method is semiexplicit in the sense that the main time evolution step is explicit whereas the symmetric projection step is implicit. We will describe the details of the method in Section 2.1 below, but let us give an overview of the method here. Given an initial point (q_0, p_0), we construct discrete dynamics $\{z_n = (q_n, p_n)\}_{n\geq 1}$ as follows: For any known $z_n = (q_n, p_n)$, we define $z_{n+1} = (q_{n+1}, p_{n+1})$ following these steps:

- $\zeta_n := (q_n, q_n, p_n, p_n) \in T^*\mathbb{R}^{2d}$;
- $\hat{\zeta}_n = (\hat{q}_n, \hat{x}_n, \hat{p}_n, \hat{y}_n) := \zeta_n + \xi_n$;
- $\hat{\zeta}_{n+1} := \hat{\Phi}_{\Delta t}(\hat{\zeta}_n)$ using an explicit extended phase space integrator $\hat{\Phi}_{\Delta t}$ such as (6);
- $\zeta_{n+1} = (q_{n+1}, q_{n+1}, p_{n+1}, p_{n+1}) := \hat{\zeta}_{n+1} + \xi_n \in \mathcal{N}$;
- $z_{n+1} := (q_{n+1}, p_{n+1})$,

where $\xi_n \in T^*\mathbb{R}^{2d}$ is a function of z_n and Δt determined by solving nonlinear equations so that $\hat{\zeta}_{n+1}$ is projected to ζ_{n+1} in $\mathcal{N}$; this is the main part of the symmetric projection step and is implicit.

The proposed method resolves those issues of the extended phase space integrators raised in the previous subsection. First, the projection step ensures $(x_n, y_n) = (q_n, p_n)$ for any $n \geq 0$—eliminating the problematic defect $(x_n - q_n, y_n - p_n)$. As we shall show in Section 2.2, this also implies that our method defines a discrete flow $\Phi_{\Delta t}\colon z_n \mapsto z_{n+1}$ in the *original* phase space $T^*\mathbb{R}^d$. We will also show in Section 2.3 that our method is symmetric assuming that $\hat{\Phi}$ is symmetric.

Our main result is that the resulting method Φ is symplectic in the *original* phase space $T^*\mathbb{R}^d$ given that the extended phase space integrator $\hat{\Phi}$ is symplectic in the extended one $T^*\mathbb{R}^{2d}$. We will prove this in Section 3 along with a geometric interpretation of the integrator.

Finally, in Section 4, we will show the implementation of the method as well as some numerical results. We will demonstrate that our method has desired orders of accuracy as well as that it preserves invariants in long-time simulations. Since the Newton-type iterations required in the projection step is very simple, the method tends to be much faster than implicit symplectic methods of the same order. The symmetric projection step being implicit, our method tends to be slower than the explicit method of Tao [27] mentioned above for low-dimensional problems. However, for higher-order methods and higher-dimensional problems, our method becomes as fast as Tao's. This demonstrates that our method resolves the issues of extended phase space integrators without sacrificing the computational efficiency for practical problems.

2. Extended Phase Space Integrators with Symmetric Projection

2.1. Definition of the Method.

Let us define a linear map

$$A\colon T^*\mathbb{R}^{2d} \cong \mathbb{R}^{4d} \to \mathbb{R}^{2d}; \qquad A(q, x, p, y) := (q - x, p - y),$$

or in the matrix representation

$$A = \begin{bmatrix} I_d & -I_d & 0 & 0 \\ 0 & 0 & I_d & -I_d \end{bmatrix}. \tag{9}$$

We see that

$$\ker A = \left\{(q, q, p, p) \in T^*\mathbb{R}^{2d} \cong \mathbb{R}^{4d} \mid q, p \in \mathbb{R}^d\right\} = \mathcal{N},$$

where $\mathcal{N}$ is defined in (4).

Then, a more detailed description of our method is the following (see also Figure 2 below):

Definition 1 (Extended phase space integrator with symmetric projection)**.** Given an extended phase space integrator $\hat{\Phi}_{\Delta t}\colon T^*\mathbb{R}^{2d} \to T^*\mathbb{R}^{2d}$ and $z_n = (q_n, p_n) \in T^*\mathbb{R}^d$,

1. $\zeta_n := (q_n, q_n, p_n, p_n)$
2. Find $\mu \in \mathbb{R}^{2d}$ such that $\hat{\Phi}_{\Delta t}(\zeta_n + A^T\mu) + A^T\mu \in \mathcal{N}$
3. $\hat{\zeta}_n := \zeta_n + A^T\mu$
4. $\hat{\zeta}_{n+1} := \hat{\Phi}_{\Delta t}(\hat{\zeta}_n)$
5. $\zeta_{n+1} = (q_{n+1}, q_{n+1}, p_{n+1}, p_{n+1}) := \hat{\zeta}_{n+1} + A^T\mu$
6. $z_{n+1} := (q_{n+1}, p_{n+1})$

Note that Steps 2–5 combined are equivalent to solving the nonlinear equations

$$\zeta_{n+1} = \hat{\Phi}_{\Delta t}(\zeta_n + A^T\mu) + A^T\mu \quad \text{and} \quad A\zeta_{n+1} = 0 \tag{10}$$

for $(\mu, \zeta_{n+1}) \in \mathbb{R}^{2d} \times T^*\mathbb{R}^{2d}$.

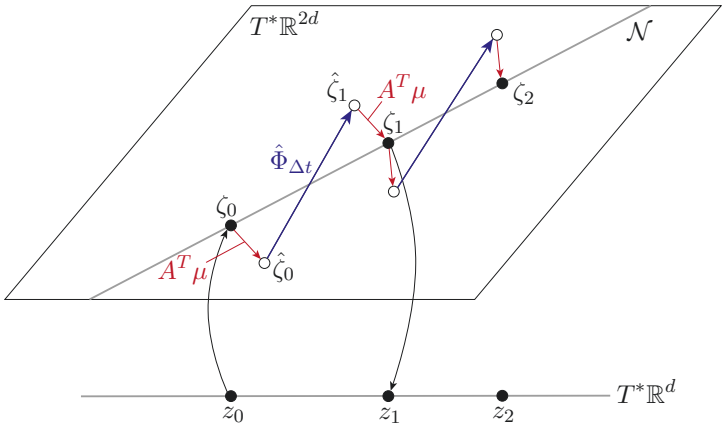

FIGURE 2. Extended phase space integrator with symmetric projection.

2.2. **Existence of Integrator.** Let us show that the above method gives rise to an integrator $\Phi_{\Delta t}\colon T^*\mathbb{R}^d \to T^*\mathbb{R}^d$ for small enough $\Delta t > 0$. To that end, let us first define

$$\iota\colon T^*\mathbb{R}^d \to \mathcal{N} \subset T^*\mathbb{R}^{2d}; \qquad (q,p) \mapsto (q,q,p,p),$$

and also, for an arbitrary $\lambda \in \mathbb{R}^{2d}$,

$$\rho_\lambda\colon T^*\mathbb{R}^{2d} \to T^*\mathbb{R}^{2d}; \qquad \zeta \mapsto \zeta + A^T\lambda.$$

In order to show that the discrete flow $\Phi_{\Delta t}\colon z_n \mapsto z_{n+1}$ exists, we need to show that, for a given $\zeta_n \in \mathcal{N}$, there exist $\zeta_{n+1} \in \mathcal{N}$ and $\mu \in \mathbb{R}^{2d}$ (a particular choice of λ from above) satisfying (10), i.e.,

$$\iota \circ \Phi_{\Delta t}(z_n) = \rho_\mu \circ \hat{\Phi}_{\Delta t} \circ \rho_\mu \circ \iota(z_n),$$

or equivalently, the diagram below commutes, where $\Psi_{\Delta t}$ will be defined in the proof of Proposition 2 to follow.

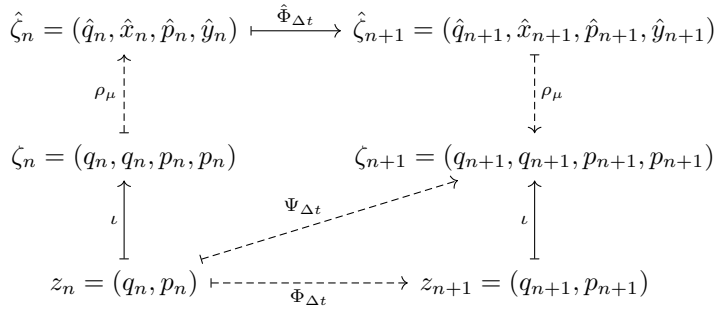

Proposition 2 (Existence of discrete flow Φ)**.** *Let $\hat{\Phi}_{(\,\cdot\,)}\colon \mathbb{R} \times T^*\mathbb{R}^{2d} \to T^*\mathbb{R}^{2d}$ be the discrete flow defined by an integrator for the extended Hamiltonian system* (3)*. For any $\bar{z}_n \in T^*\mathbb{R}^d$, there exist*

- *a neighborhood U of $\bar{z}_n$ in $T^*\mathbb{R}^d$;*
- *$\varepsilon > 0$;*
- *$\mu_{(\,\cdot\,)}\colon (-\varepsilon, \varepsilon) \times U \to \mathbb{R}^{2d}$ and $\Phi_{(\,\cdot\,)}\colon (-\varepsilon, \varepsilon) \times U \to T^*\mathbb{R}^d$*

such that, for any $\Delta t \in (-\varepsilon, \varepsilon)$ and any $z_n \in U$,

$$\iota \circ \Phi_{\Delta t}(z_n) = \hat{\Phi}_{\Delta t}\big(\iota(z_n) + A^T \mu_{\Delta t}(z_n)\big) + A^T \mu_{\Delta t}(z_n).$$

Proof. Let us define

$$F\colon (\mathbb{R} \times T^*\mathbb{R}^d) \times (T^*\mathbb{R}^{2d} \times \mathbb{R}^{2d}) \to T^*\mathbb{R}^{2d} \times \mathbb{R}^{2d}$$
$$F((h, z_n), (\zeta, \lambda)) := \begin{bmatrix} \zeta - \hat{\Phi}_h\big(\iota(z_n) + A^T\lambda\big) - A^T\lambda \\ A\zeta \end{bmatrix}.$$

Then the Jacobian

$$\frac{\partial F}{\partial(\zeta, \lambda)}((0, \bar{z}_n), (\iota(\bar{z}_n), 0)) = \begin{bmatrix} I_{2d} & -2A^T \\ A & 0 \end{bmatrix}$$

is invertible because A—defined in (9)—is full-rank. Therefore, by the Implicit Function Theorem, there exist a neighborhood $U \subset T^*\mathbb{R}^d$ of $\bar{z}_n$, a positive number $\varepsilon > 0$, and

$$\Psi_{(\,\cdot\,)}\colon (-\varepsilon, \varepsilon) \times U \to T^*\mathbb{R}^{2d}, \qquad \mu_{(\,\cdot\,)}\colon (-\varepsilon, \varepsilon) \times U \to \mathbb{R}^{2d}$$

such that, for any $(\Delta t, z_n) \in (-\varepsilon, \varepsilon) \times U$,

$$F((\Delta t, z_n), (\Psi_{\Delta t}(z_n), \mu_{\Delta t}(z_n))) = 0,$$

that is,

$$\Psi_{\Delta t}(z_n) = \hat{\Phi}_{\Delta t}\big(\iota(z_n) + A^T \mu_{\Delta t}(z_n)\big) + A^T \mu_{\Delta t}(z_n), \qquad A\Psi_{\Delta t}(z_n) = 0.$$

However, since the second equality says $\Psi_{\Delta t}(z_n) \in \mathcal{N}$, there exists

$$\Phi_{\Delta t}\colon U \to T^*\mathbb{R}^d \quad \text{such that} \quad \Psi_{\Delta t}(z_n) = \iota \circ \Phi_{\Delta t}(z_n). \qquad \square$$

2.3. **Symmetry and Order of Φ.** We can also show that our method Φ is symmetric assuming that the extended phase space integrator $\hat{\Phi}$ is symmetric:

Proposition 3 (Symmetry and order of Φ)**.** *If the extended phase space integrator $\hat{\Phi}$ is symmetric, then the integrator Φ defined in Proposition 2 is symmetric, i.e., $\Phi_{\Delta t}^{-1} = \Phi_{-\Delta t}$ for any $\Delta t \in (-\varepsilon, \varepsilon)$ with $\varepsilon > 0$ defined in Proposition 2. Moreover, Φ has the same order of accuracy as $\hat{\Phi}$.*

Proof. Let us first prove the symmetry. It is proved in Hairer et al. [11, p. 163] that a symmetric method combined with the symmetric projection method yields a symmetric method. In our setting, this implies that $\phi_{\Delta t} \colon \mathcal{N} \to \mathcal{N}$ defined by $\zeta_n \mapsto \zeta_{n+1}$ (see the diagram below) is symmetric, i.e., $\phi_{-\Delta t} = \phi_{\Delta t}^{-1}$.

$$\begin{array}{ccc} \zeta_n = (q_n, q_n, p_n, p_n) & \underset{\phi_{\Delta t}^{-1}=\phi_{-\Delta t}}{\overset{\phi_{\Delta t}}{\rightleftarrows}} & \zeta_{n+1} = (q_{n+1}, q_{n+1}, p_{n+1}, p_{n+1}) \\ \updownarrow & & \updownarrow \\ z_n = (q_n, p_n) & \underset{\Phi_{\Delta t}}{\overset{\Phi_{\Delta t}^{-1}}{\rightleftarrows}} & z_{n+1} = (q_{n+1}, p_{n+1}) \end{array}$$

However, ϕ and Φ are essentially the same map because one may identify ζ_n and ζ_{n+1} with z_n and z_{n+1}, respectively, as shown in the diagram. In other words, the above diagram commutes. Thus the symmetry of ϕ implies that of Φ.

For the order of accuracy, again a result from [11, p. 163] applied to our setting implies that ϕ solves the extended system (3) on $\mathcal{N}$ with the same order of accuracy as $\hat{\Phi}$. However, as we have discussed in Section 1.2, the extended system (3) on $\mathcal{N}$ is two identical copies of the original system (1). Therefore, this implies that Φ solves (1) with the same order of accuracy as well. □

2.4. **Is $\Phi_{\Delta t}$ Symplectic?** Here we shall perform some calculations to show that

$$\mathbf{d}q_{n+1} \wedge \mathbf{d}p_{n+1} = \mathbf{d}q_n \wedge \mathbf{d}p_n.$$

One may consider the calculations to follow as a proof of symplecticity. However, the argument to follow hardly reveals the geometry behind it because it is somewhat intricate. Therefore, in Section 3.2 below, we shall present the underlying geometry of the method, and give a more geometrically sound proof of the symplecticity than what follows.

Let us write $\mu = (\mu_1, \mu_2) \in \mathbb{R}^{2d}$ with $\mu_1, \mu_2 \in \mathbb{R}^d$. Then we have

(11)
$$\zeta_{n+1} = (q_{n+1}, q_{n+1}, p_{n+1}, p_{n+1}) = (\hat{q}_{n+1} + \mu_1,\, \hat{x}_{n+1} - \mu_1,\, \hat{p}_{n+1} + \mu_2,\, \hat{y}_{n+1} - \mu_2),$$

and so

$$q_{n+1} - \hat{q}_{n+1} = \mu_1 = \hat{x}_{n+1} - q_{n+1}, \qquad p_{n+1} - \hat{p}_{n+1} = \mu_2 = \hat{y}_{n+1} - p_{n+1}.$$

Therefore,

$$q_{n+1} = \frac{1}{2}(\hat{q}_{n+1} + \hat{x}_{n+1}), \qquad p_{n+1} = \frac{1}{2}(\hat{p}_{n+1} + \hat{y}_{n+1}).$$

and thus

(12)
$$\begin{aligned}\mathbf{d}q_{n+1}\wedge\mathbf{d}p_{n+1} = \frac{1}{4}\big(&\mathbf{d}\hat{q}_{n+1}\wedge\mathbf{d}\hat{p}_{n+1} + \mathbf{d}\hat{x}_{n+1}\wedge\mathbf{d}\hat{y}_{n+1}\\ &+ \mathbf{d}\hat{q}_{n+1}\wedge\mathbf{d}\hat{y}_{n+1} + \mathbf{d}\hat{x}_{n+1}\wedge\mathbf{d}\hat{p}_{n+1}\big)\end{aligned}$$

$$= \frac{1}{4}(\mathbf{d}\hat{q}_n\wedge\mathbf{d}\hat{p}_n + \mathbf{d}\hat{x}_n\wedge\mathbf{d}\hat{y}_n + \mathbf{d}\hat{q}_{n+1}\wedge\mathbf{d}\hat{y}_{n+1} + \mathbf{d}\hat{x}_{n+1}\wedge\mathbf{d}\hat{p}_{n+1}), \tag{13}$$

where we also used the symplecticity of $\hat{\Phi}_{\Delta t}\colon \hat{\zeta}_n \mapsto \hat{\zeta}_{n+1}$ on the extended phase space $T^*\mathbb{R}^{2d}$, i.e.,

$$\mathbf{d}\hat{q}_{n+1}\wedge\mathbf{d}\hat{p}_{n+1} + \mathbf{d}\hat{x}_{n+1}\wedge\mathbf{d}\hat{y}_{n+1} = \mathbf{d}\hat{q}_n\wedge\mathbf{d}\hat{p}_n + \mathbf{d}\hat{x}_n\wedge\mathbf{d}\hat{y}_n. \tag{14}$$

Now, from (11), we also have

$$\begin{aligned}\hat{x}_{n+1} - \hat{q}_{n+1} &= (q_{n+1}+\mu_1) - (q_{n+1}-\mu_1) = 2\mu_1,\\ \hat{y}_{n+1} - \hat{p}_{n+1} &= (p_{n+1}+\mu_2) - (p_{n+1}-\mu_2) = 2\mu_2.\end{aligned}$$

On the other hand, recall that we also have

$$\hat{\zeta}_n = (\hat{q}_n, \hat{x}_n, \hat{p}_n, \hat{y}_n) = (q_n+\mu_1,\, q_n-\mu_1,\, p_n+\mu_2,\, p_n-\mu_2), \tag{15}$$

and so, similarly,

$$\hat{q}_n - \hat{x}_n = (q_n+\mu_1) - (q_n-\mu_1) = 2\mu_1, \quad \hat{p}_n - \hat{y}_n = (p_n+\mu_2) - (p_n-\mu_2) = 2\mu_2.$$

Therefore, we obtain

$$\hat{x}_{n+1} - \hat{q}_{n+1} = \hat{q}_n - \hat{x}_n, \qquad \hat{y}_{n+1} - \hat{p}_{n+1} = \hat{p}_n - \hat{y}_n,$$

and so

$$\mathbf{d}(\hat{x}_{n+1} - \hat{q}_{n+1})\wedge\mathbf{d}(\hat{y}_{n+1} - \hat{p}_{n+1}) = \mathbf{d}(\hat{q}_n - \hat{x}_n)\wedge\mathbf{d}(\hat{p}_n - \hat{y}_n).$$

Subtracting (14) from this identity,

$$\mathbf{d}\hat{q}_{n+1}\wedge\mathbf{d}\hat{y}_{n+1} + \mathbf{d}\hat{x}_{n+1}\wedge\mathbf{d}\hat{p}_{n+1} = \mathbf{d}\hat{q}_n\wedge\mathbf{d}\hat{y}_n + \mathbf{d}\hat{x}_n\wedge\mathbf{d}\hat{p}_n.$$

Therefore, (12) now gives

$$\mathbf{d}q_{n+1}\wedge\mathbf{d}p_{n+1} = \frac{1}{4}(\mathbf{d}\hat{q}_n\wedge\mathbf{d}\hat{p}_n + \mathbf{d}\hat{x}_n\wedge\mathbf{d}\hat{y}_n + \mathbf{d}\hat{q}_n\wedge\mathbf{d}\hat{y}_n + \mathbf{d}\hat{x}_n\wedge\mathbf{d}\hat{p}_n),$$

On the other hand, (15) also gives

$$q_n = \frac{1}{2}(\hat{q}_n + \hat{x}_n), \qquad p_n = \frac{1}{2}(\hat{p}_n + \hat{y}_n),$$

and thus

$$\mathbf{d}q_n\wedge\mathbf{d}p_n = \frac{1}{4}(\mathbf{d}\hat{q}_n\wedge\mathbf{d}\hat{p}_n + \mathbf{d}\hat{x}_n\wedge\mathbf{d}\hat{y}_n + \mathbf{d}\hat{q}_n\wedge\mathbf{d}\hat{y}_n + \mathbf{d}\hat{x}_n\wedge\mathbf{d}\hat{p}_n).$$

As a result, we obtain

$$\mathbf{d}q_{n+1}\wedge\mathbf{d}p_{n+1} = \mathbf{d}q_n\wedge\mathbf{d}p_n.$$

3. Geometry of Integrator and Symplecticity

As mentioned at the beginning of Section 2.4, the calculations performed above hardly reveals the geometry involved in the method in proving the symplecticity of the method. In this section, we first provide a geometric interpretation of the method. This will help us construct a more natural proof of symplecticity.

3.1. **Geometry of Integrator $\Phi_{\Delta t}$.** Building on Proposition 2, we first would like to write our integrator $\Phi_{\Delta t}$ as a composition of some maps.

Let us first consider the step

$$\zeta_n \mapsto \hat{\zeta}_n = \zeta_n + A^T\mu. \tag{16}$$

We can show that $\hat{\zeta}_n$ is in a certain submanifold of $T^*\mathbb{R}^{2d}$:

Lemma 4. *Define*

$$\mathcal{M} := \Big\{\zeta \in T^*\mathbb{R}^{2d} \mid A \circ \hat{\Phi}_{\Delta t}(\zeta) = -A\zeta\Big\}, \tag{17}$$

where $\hat{\Phi}_{\Delta t}$ is written in terms of the coordinates (q, x, p, y). Then:

(i) For a small enough $|\Delta t| > 0$, $\mathcal{M}$ is a $2d$-dimensional submanifold of $T^*\mathbb{R}^{2d} \cong \mathbb{R}^{4d}$.

(ii) $\hat{\zeta}_n \in \mathcal{M}$.

Proof. (i) Define

$$G\colon T^*\mathbb{R}^{2d} \cong \mathbb{R}^{4d} \to \mathbb{R}^{2d}; \qquad G(\zeta) := A \circ \hat{\Phi}_{\Delta t}(\zeta) + A\zeta.$$

Then $\mathcal{M} = G^{-1}(0)$. So it suffices to show that the following differential of G is full-rank:

$$DG(\zeta) = A \circ D\hat{\Phi}_{\Delta t}(\zeta) + A = A\big(D\hat{\Phi}_{\Delta t}(\zeta) + I_{4d}\big).$$

Since $D\hat{\Phi}_0 = I_{4d}$, for a small enough $|\Delta t| > 0$, $D\hat{\Phi}_{\Delta t}(\zeta) + I_{4d}$ is invertible. However, since A is full-rank, this implies that $DG(\zeta)$ is full-rank for any $\zeta \in T^*\mathbb{R}^{2d}$ as well.

(ii) In view of Definition 1 and (10), $\hat{\zeta}_n$ satisfies

$$\zeta_{n+1} = \hat{\Phi}_{\Delta t}\big(\hat{\zeta}_n\big) + A^T\mu \quad \text{and} \quad A\zeta_{n+1} = 0.$$

However, since (16) gives $A^T\mu = \hat{\zeta}_n - \zeta_n$, we have

$$\zeta_{n+1} = \hat{\Phi}_{\Delta t}\big(\hat{\zeta}_n\big) + \hat{\zeta}_n - \zeta_n \quad \text{and} \quad A\zeta_{n+1} = 0.$$

Multiplying A from the left to the first equality and noting that $\zeta_n, \zeta_{n+1} \in \mathcal{N} = \ker A$, we obtain

$$0 = A \circ \hat{\Phi}_{\Delta t}\big(\hat{\zeta}_n\big) + A\hat{\zeta}_n,$$

that is, $\hat{\zeta}_n \in \mathcal{M}$. □

As a result, using the map $\mu_{(\,\cdot\,)}\colon (-\varepsilon, \varepsilon) \times U \to T^*\mathbb{R}^{2d}$ introduced in Proposition 2, this step is described by the map

$$\sigma_{\Delta t}\colon \mathcal{N} \to \mathcal{M}; \qquad (q, q, p, p) \mapsto (q, q, p, p) + A^T\mu_{\Delta t}(q, p).$$

We shall also need the following embedding later:

$$i_{\mathcal{M}}\colon \mathcal{M} \hookrightarrow T^*\mathbb{R}^{2d}.$$

Let us next look at the step

$$\hat{\zeta}_{n+1} \mapsto \zeta_{n+1} = \hat{\zeta}_{n+1} + A^T\mu,$$

or

$$(\hat{q}_{n+1}, \hat{x}_{n+1}, \hat{p}_{n+1}, \hat{y}_{n+1}) \mapsto (\hat{q}_{n+1} + \mu_1,\, \hat{x}_{n+1} - \mu_1,\, \hat{p}_{n+1} + \mu_2,\, \hat{y}_{n+1} - \mu_2).$$

Notice that, since $\zeta_{n+1} \in \mathcal{N}$, we may equate the first two terms as well as the last two on the right-hand side to have

$$\mu_1 = \frac{1}{2}(\hat{x}_{n+1} - \hat{q}_{n+1}) \qquad \mu_2 = \frac{1}{2}(\hat{y}_{n+1} - \hat{p}_{n+1}).$$

Therefore, one may rewrite this step as

$$(\hat{q}_{n+1}, \hat{x}_{n+1}, \hat{p}_{n+1}, \hat{y}_{n+1}) \mapsto \left(\frac{\hat{q}_{n+1} + \hat{x}_{n+1}}{2}, \frac{\hat{q}_{n+1} + \hat{x}_{n+1}}{2}, \frac{\hat{p}_{n+1} + \hat{y}_{n+1}}{2}, \frac{\hat{p}_{n+1} + \hat{y}_{n+1}}{2} \right).$$

This motivates us to define the map

$$\kappa \colon T^*\mathbb{R}^{2d} \to \mathcal{N} \subset T^*\mathbb{R}^{2d}; \qquad (q, x, p, y) \mapsto \left(\frac{q+x}{2}, \frac{q+x}{2}, \frac{p+y}{2}, \frac{p+y}{2} \right).$$

so that

$$\zeta_{n+1} = \kappa(\hat{\zeta}_n).$$

Finally, in order to describe the last step

$$\zeta_{n+1} = (q_n, q_n, p_n, p_n) \mapsto z_n = (q_n, p_n),$$

let us define

$$\varpi \colon \mathcal{N} \to T^*\mathbb{R}^d; \qquad (q, q, p, p) \mapsto (q, p).$$

Putting all of the maps together, we have the diagram below for our integrator Φ.

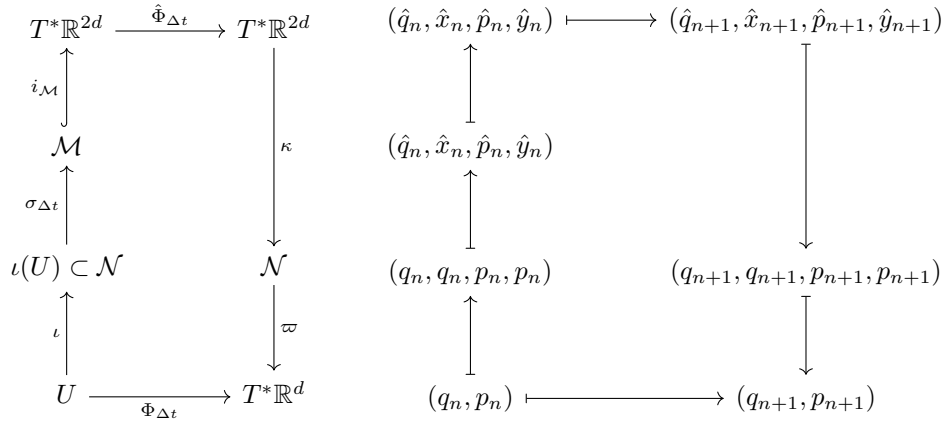

In other words, we may write the integrator $\Phi_{\Delta t}$ as follows:

$$\Phi_{\Delta t} = \varpi \circ \kappa \circ \hat{\Phi}_{\Delta t} \circ i_{\mathcal{M}} \circ \sigma_{\Delta t} \circ \iota. \tag{18}$$

3.2. **Symplecticity of $\Phi_{\Delta t}$.** Now we are ready to prove our main result:

Theorem 5 (Symplecticity of $\Phi_{\Delta t}$)**.** *The integrator $\Phi_{\Delta t} \colon T^*\mathbb{R}^d \to T^*\mathbb{R}^d$ is symplectic, i.e.,*

$$\Phi_{\Delta t}^* \Omega = \Omega.$$

Let us first prove the following lemma:

Lemma 6. *Let us define the following 2-form on $T^*\mathbb{R}^{2d}$:*

$$\Xi := \mathbf{d}q \wedge \mathbf{d}y + \mathbf{d}x \wedge \mathbf{d}p.$$

Then

$$\kappa^* \varpi^* \Omega = \frac{1}{4}(\hat{\Omega} + \Xi) \tag{19}$$

and

$$i_{\mathcal{M}}^{*}\hat{\Phi}_{\Delta t}^{*}\Xi = i_{\mathcal{M}}^{*}\Xi. \tag{20}$$

Proof. Let us first prove (19). We may write

$$\varpi \circ \kappa(q,x,p,y) = \left(\frac{q+x}{2}, \frac{p+y}{2}\right).$$

So the pull-back of Ω by this map yields

$$\begin{aligned}
\kappa^{*}\varpi^{*}\Omega &= (\varpi\circ\kappa)^{*}\Omega \\
&= \frac{1}{4}(\mathbf{d}q + \mathbf{d}x)\wedge(\mathbf{d}p+\mathbf{d}y) \\
&= \frac{1}{4}(\mathbf{d}q\wedge\mathbf{d}p + \mathbf{d}x\wedge\mathbf{d}y + \mathbf{d}q\wedge\mathbf{d}y + \mathbf{d}x\wedge\mathbf{d}p) \\
&= \frac{1}{4}(\hat{\Omega}+\Xi).
\end{aligned}$$

Let us next prove (20). It suffices to show that, for any $\zeta\in\mathcal{M}$ and any tangent vectors $v,w\in T_{\zeta}\mathcal{M}$,

$$(\hat{\Phi}_{\Delta t}^{*}\Xi)_{\zeta}(v,w) = \Xi_{\zeta}(v,w).$$

Let us identify $v,w\in T_{\zeta}\mathcal{M}$ with vectors in $\mathbb{R}^{4d}$ written in terms of the coordinates

$$\left\{ \frac{\partial}{\partial q}\Big|_{\zeta}, \frac{\partial}{\partial x}\Big|_{\zeta}, \frac{\partial}{\partial p}\Big|_{\zeta}, \frac{\partial}{\partial y}\Big|_{\zeta} \right\}$$

for $T_{\zeta}(T^{*}\mathbb{R}^{2d})\cong\mathbb{R}^{4d}$. In view of the definition (17) of the submanifold $\mathcal{M}$, one sees that $v,w\in T_{\zeta}\mathcal{M}\cong\mathbb{R}^{4d}$ satisfy

$$A\circ D\hat{\Phi}_{\Delta t}(\zeta)v = -Av, \qquad A\circ D\hat{\Phi}_{\Delta t}(\zeta)w = -Aw.$$

Now, we may write, using the definition of Ξ,

$$\Xi_{\zeta}(v,w) = v^{T}\mathbb{X}w \quad \text{with} \quad \mathbb{X} := \begin{bmatrix} 0 & 0 & 0 & I_d \\ 0 & 0 & I_d & 0 \\ 0 & -I_d & 0 & 0 \\ -I_d & 0 & 0 & 0 \end{bmatrix}.$$

Let us set, for any $d\in\mathbb{N}$,

$$\mathbb{J}_{2d} := \begin{bmatrix} 0 & I_d \\ -I_d & 0 \end{bmatrix}.$$

Then it is a straightforward calculation to see that

$$A^{T}\mathbb{J}_{2d}A = \begin{bmatrix} 0 & 0 & I_d & -I_d \\ 0 & 0 & -I_d & I_d \\ -I_d & I_d & 0 & 0 \\ I_d & -I_d & 0 & 0 \end{bmatrix} = \mathbb{J}_{4d} - \mathbb{X} \iff \mathbb{X} = \mathbb{J}_{4d} - A^{T}\mathbb{J}_{2d}A.$$

Notice also that $\hat{\Phi}_{\Delta t}\colon T^{*}\mathbb{R}^{2d}\to T^{*}\mathbb{R}^{2d}$ is symplectic, i.e.,

$$D\hat{\Phi}_{\Delta t}(\zeta)^{T}\mathbb{J}_{4d}D\Phi_{\Delta t}(\zeta) = \mathbb{J}_{4d}.$$

Therefore, we have

$$\begin{aligned}(\hat{\Phi}^*_{\Delta t}\Xi)_\zeta(v,w) &= (D\hat{\Phi}_{\Delta t}(\zeta)v)^T\mathbb{X}(D\hat{\Phi}_{\Delta t}(\zeta)w)\\ &= v^T D\hat{\Phi}_{\Delta t}(\zeta)^T\mathbb{J}_{4d}D\hat{\Phi}_{\Delta t}(\zeta)w - (v^T D\hat{\Phi}_{\Delta t}(\zeta)^T)A^T\mathbb{J}_{2d}A(D\hat{\Phi}_{\Delta t}(\zeta)w)\\ &= v^T\mathbb{J}_{4d}w - (A\circ D\hat{\Phi}_{\Delta t}(\zeta)v)^T\mathbb{J}_{2d}(A\circ D\hat{\Phi}_{\Delta t}(\zeta)w)\\ &= v^T\mathbb{J}_{4d}w - (-Av)^T\mathbb{J}_{2d}(-Aw)\\ &= v^T\mathbb{J}_{4d}w - v^TA^T\mathbb{J}_{2d}Aw\\ &= v^T\mathbb{J}_{4d}w - v^T(\mathbb{J}_{4d}-\mathbb{X})w\\ &= v^T\mathbb{X}w\\ &= \Xi_\zeta(v,w).\end{aligned}$$

□

Now we are ready to prove the main result.

Proof of Theorem 5. Since we may write

$$i_{\mathcal{M}}\circ\sigma_{\Delta t}\circ\iota(q,p) = (q+\mu_1,\, q-\mu_1,\, p+\mu_2,\, p-\mu_2),$$

we have

$$\begin{aligned}\iota^*\sigma^*_{\Delta t}i^*_{\mathcal{M}}(\hat{\Omega}+\Xi) &= (\mathbf{d}q+\mathbf{d}\mu_1)\wedge(\mathbf{d}p+\mathbf{d}\mu_2) + (\mathbf{d}q-\mathbf{d}\mu_1)\wedge(\mathbf{d}p-\mathbf{d}\mu_2)\\ &\quad + (\mathbf{d}q+\mathbf{d}\mu_1)\wedge(\mathbf{d}p-\mathbf{d}\mu_2) + (\mathbf{d}q-\mathbf{d}\mu_1)\wedge(\mathbf{d}p+\mathbf{d}\mu_2)\\ &= 4\mathbf{d}q\wedge\mathbf{d}p\\ &= 4\Omega.\end{aligned}$$

Therefore, using the definition (18), the equalities (19) and (20) from Lemma 6, the symplecticity of $\hat{\Phi}_{\Delta t}$ with respect to $\hat{\Omega}$, and the above equality, we have

$$\begin{aligned}\Phi^*_{\Delta t}\Omega &= \iota^*\sigma^*_{\Delta t}i^*_{\mathcal{M}}\hat{\Phi}^*_{\Delta t}\kappa^*\varpi^*\Omega\\ &= \frac{1}{4}\iota^*\sigma^*_{\Delta t}i^*_{\mathcal{M}}\hat{\Phi}^*_{\Delta t}(\hat{\Omega}+\Xi)\\ &= \frac{1}{4}\iota^*\sigma^*_{\Delta t}i^*_{\mathcal{M}}(\hat{\Omega}+\Xi)\\ &= \Omega.\end{aligned}$$

□

4. Implementation and Numerical Results

4.1. **Implementation.** Our base 2nd-order method uses the extended phase space integrator (6) of Pihajoki [21] using the Strang splitting. We can construct higher-order extended phase space integrators from (6) using the symmetric Triple Jump composition (see [7, 9, 25, 33]; also Hairer et al. [11, Example II.4.2]). For example, denoting the above 2nd-order method in (6) by $\hat{\Phi}^{(2)}_{\Delta t}$, we recursively construct an n^{th}-order (n being even) method as follows:

$$\hat{\Phi}^{(n)}_{\Delta t} := \hat{\Phi}^{(n-2)}_{\gamma_3\Delta t}\circ\hat{\Phi}^{(n-2)}_{\gamma_2\Delta t}\circ\hat{\Phi}^{(n-2)}_{\gamma_1\Delta t}, \tag{21}$$

where

$$\gamma_1 = \gamma_3 := \frac{1}{2-2^{1/(n-1)}}, \qquad \gamma_2 := -\frac{2^{1/(n-1)}}{2-2^{1/(n-1)}}.$$

This results in a $3^{n/2}$-stage method of order n. For example, the 4th order Triple Jump composition is a 9-stage method, whereas the 6th-order method has 27 stages.

Another composition technique we have considered is the fractals method of Suzuki [25] (see also [11, Example II.4.3]), i.e., instead of (21),

$$\hat{\Phi}^{(n)}_{\Delta t} := \hat{\Phi}^{(n-2)}_{\gamma_5 \Delta t} \circ \hat{\Phi}^{(n-2)}_{\gamma_4 \Delta t} \circ \hat{\Phi}^{(n-2)}_{\gamma_3 \Delta t} \circ \hat{\Phi}^{(n-2)}_{\gamma_2 \Delta t} \circ \hat{\Phi}^{(n-2)}_{\gamma_1 \Delta t} \tag{22}$$

with

$$\gamma_1 = \gamma_2 = \gamma_4 = \gamma_5 := \frac{1}{4 - 4^{1/(n-1)}}, \qquad \gamma_3 := -\frac{4^{1/(n-1)}}{4 - 4^{1/(n-1)}}.$$

We also used Yoshida's method [33] (see also [11, Section V.3.2]), which is a 6^{th}-order symmetric composition technique with 7 stages.

For the symmetric projection step, recall that we need to solve the nonlinear equations

$$F_{\Delta t}(\zeta_{n+1}, \mu) := \begin{bmatrix} \zeta_{n+1} - \hat{\Phi}_{\Delta t}(\zeta_n + A^T \mu) - A^T \mu \\ A \zeta_{n+1} \end{bmatrix} = 0$$

for (ζ_{n+1}, μ). However, one may eliminate ζ_{n+1} to have the following nonlinear equation for μ:

$$f_{\Delta t}(\mu) := A\Big(\hat{\Phi}_{\Delta t}(\zeta_n + A^T \mu) + A^T \mu\Big) = 0. \tag{23}$$

Its Jacobian is

$$Df_{\Delta t}(\mu) = A\, D\hat{\Phi}_{\Delta t}(\zeta_n + A^T \mu)\, A^T + AA^T,$$

and becomes very simple for $\Delta t = 0$: Noting that $AA^T = 2I_{2d}$, we have

$$Df_0(\mu) = 2AA^T = 4I_{2d}.$$

As suggested by Hairer et al. [11, Section V.4.1], we exploit this simple structure of the Jacobian to construct the simplified Newton approximation

$$\mu^{(k+1)} = \mu^{(k)} - (Df_0)^{-1} f_{\Delta t}\big(\mu^{(k)}\big) = \mu^{(k)} - \frac{1}{4} f_{\Delta t}\big(\mu^{(k)}\big), \tag{24}$$

where we start with $\mu^{(0)} = 0$. As we shall see in Section 4.5, these simplified Newton iterations tend to converge quickly with a reasonable tolerance ϵ imposed so it stops after N iterations

$$\Big\| \mu^{(N+1)} - \mu^{(N)} \Big\| < \epsilon, \tag{25}$$

and we set $\mu = \mu^{(N)}$.

4.2. **Broyden's Method.** While the above simplified Newton method (24) is computationally efficient and works well in most of the examples we shall show below, it is not clear if one can prove that such a method indeed converges to an actual solution of the nonlinear equations. In fact, as we shall see in Appendix A.3 (Table 6), the method seems to occasionally fail to converge after a reasonable number of iterations ($N \leq 100$ in our simulations) depending on the problem and the values of Δt and ϵ.

Therefore, one may instead use the following quasi-Newton method called Broyden's method [2]:

$$\mu^{(k+1)} = \mu^{(k)} - J_k^{-1} f_{\Delta t}\big(\mu^{(k)}\big), \tag{26a}$$

where $\{J_k\}_{k\geq 0}$ are approximations to $\{Df_{\Delta t}(\mu^{(k)})\}_{k\geq 0}$ defined by the initial guess $J_0 := Df_0(\mu^{(0)}) = 4I_{2d}$ and the updates

$$J_k = J_{k-1} + \frac{\Delta f^{(k)} - J_{k-1}\Delta\mu^{(k)}}{\left\|\Delta\mu^{(k)}\right\|^2}\big(\Delta\mu^{(k)}\big)^T \quad \text{for} \quad k \geq 1$$

with $\Delta f^{(k)} := f(\mu^{(k)}) - f(\mu^{(k-1)})$ and $\Delta\mu^{(k)} := \mu^{(k)} - \mu^{(k-1)}$. This guarantees a q-quadratic convergence to an actual solution μ_* in our setting, assuming that $\mu^{(0)}$ and $J_0 = Df_0(\mu^{(0)})$ are close enough to μ_* and $Df_{\Delta t}(\mu_*)$, respectively; see, e.g., Gay [10] and Mannel [16] for details. This condition is satisfied if Δt is taken small enough. Indeed, notice that setting $\Delta t = 0$ yields $\mu_* = 0$ and also that μ_* depends smoothly on Δt (assuming that the Hamiltonian H is smooth). Therefore, if Δt is taken small enough, then $\mu_* \approx \mu^{(0)}$ and so $Df_{\Delta t}(\mu_*) \approx Df_0(\mu^{(0)})$ as well.

As Broyden [2] suggested, it is computationally efficient to calculate the inverse J_{k+1}^{-1} directly from J_k^{-1} using the Sherman–Morrison formula as follows:

$$J_k^{-1} = J_{k-1}^{-1} + \frac{\Delta\mu^{(k)} - J_{k-1}^{-1}\Delta f^{(k)}}{\big(\Delta\mu^{(k)}\big)^T J_{k-1}^{-1}\Delta f^{(k)}}\big(\Delta\mu^{(k)}\big)^T J_{k-1}^{-1}. \tag{26b}$$

The update (26a) along with (26b) is the well-known *good Broyden's method*.

As we shall show in Appendix A, Broyden's method offers an improvement in convergence and works well even for those cases where the simplified method (24) seems to fail to converge in a reasonable number of iterations.

4.3. **Order of Method.** As proved in Proposition 3, our method Φ has the same order of accuracy as the extended integrator $\hat{\Phi}$ used. We would like to numerically demonstrate this result using the following simple example: Consider the Hamiltonian system (1) on $T^*\mathbb{R}$ with the Hamiltonian

$$H(q,p) = \frac{1}{2}\big(q^2+1\big)\big(p^2+1\big) \tag{27}$$

with initial condition $(q(0), p(0)) = (-3, 0)$; this is exact solvable as shown in Tao [27].

We implemented our proposed semiexplicit method of orders 2, 4, and 6 using the Triple Jump (21) as well as 4^{th}- and 6^{th}-order methods using Suzuki's composition (22) and Yoshida's 6^{th}-order composition mentioned above.

For comparison, we also used the 2^{nd}- and 4^{th}-order Gauss–Legendre methods (see, e.g., Hairer et al. [11, Section II.1.3] and Leimkuhler and Reich [12, Table 6.4 on p. 154]); its 2^{nd}-order method is commonly known as the Implicit Midpoint method, whereas we refer to the 4^{th}-order method as the IRK4 for short here. We note that these methods are known to be symplectic; see, e.g., [11, Theorem VI.4.2] and [12, Section 6.3.1].

Figure 3 shows how the maximum relative error in the Hamiltonian depends on the time step for our method along with Tao's method [27] of the same orders, as well as the Gauss–Legendre methods. We observe that our semiexplicit method exhibits the desired orders of accuracy. Note that the errors of the 6^{th}-order methods for smaller time steps seem to be affected by the errors in the projection step, where the tolerance is $\epsilon = 10^{-15}$ here. Notice also that our method is consistently more accurate than Tao's of the same order.

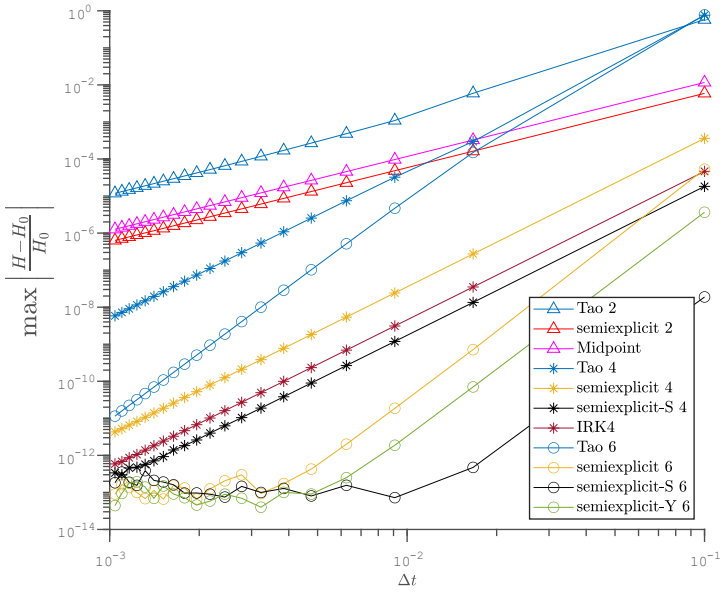

FIGURE 3. Maximum relative error in Hamiltonian (27) (compared to initial value H_0) for different time steps with various methods: Tao [27] (see (8)) with $\omega = 20$ using Triple Jump (21); proposed semiexplicit method with Triple Jump, Suzuki's and Yoshida's compositions; 2^{nd}-order Implicit Midpoint and the 4^{th}-order Gauss–Legendre method (IRK4). Simulations with terminal time $T = 100$ and with a tolerance of $\epsilon = 10^{-15}$ for the projection step were taken to calculate the maximum absolute relative error of Hamiltonian H for time steps $\Delta t \in [0.001, 0.1]$.

4.4. **Preservation of Invariants.** Next we would like to address the long-time preservation of invariants of the system. Before getting into the comparison of our method with Tao's [27], let us first mention the main factor that affects the preservation of invariants. As mentioned in Section 1.4, the main issue of the original extended phase space integrator of Pihajoki [21] is the growth of the defect $(x - q, y - p)$. Tao's modification seems to suppress this growth. However, as we shall see below, the defect seems to affect the error of the the invariants.

Let us numerically demonstrate the behavior of the defect with an example. Consider the following finite-dimensional approximation to the nonlinear Schrödinger equation (NLS) equation (see Colliander et al. [5]) used in Tao [27]. It is a Hamiltonian system (1) with $d = N$ and the non-separable Hamiltonian

(28)
$$H(q,p) = \frac{1}{4}\sum_{i=1}^{N}\left(q_i^2+p_i^2\right)^2 - \sum_{i=2}^{N}\left(p_{i-1}^2p_i^2 + q_{i-1}^2q_i^2 - q_{i-1}^2p_i^2 - p_{i-1}^2q_i^2 + 4p_{i-1}p_iq_{i-1}q_i\right).$$

We note that this system has another invariant

(29)
$$I(q,p) := \sum_{i=1}^{N}\left(q_i^2+p_i^2\right)$$

called the total mass. Following Tao [27], we set $N = 5$, $\omega = 100$, and $q(0) = (3, 0.01, 0.01, 0.01, 0.01)$ and $p(0) = (1, 0, 0, 0, 0)$. Figure 4 shows how the Euclidean norm $\|(q, p) - (x, y)\|$ of the defect changes with time. Note that higher-order methods of Tao (8) are constructed by the Tripe Jump composition (21) as well. One can see that, compared to Pihajoki's integrator (6), Tao's middle step is able to successfully suppress the defect into small oscillations.

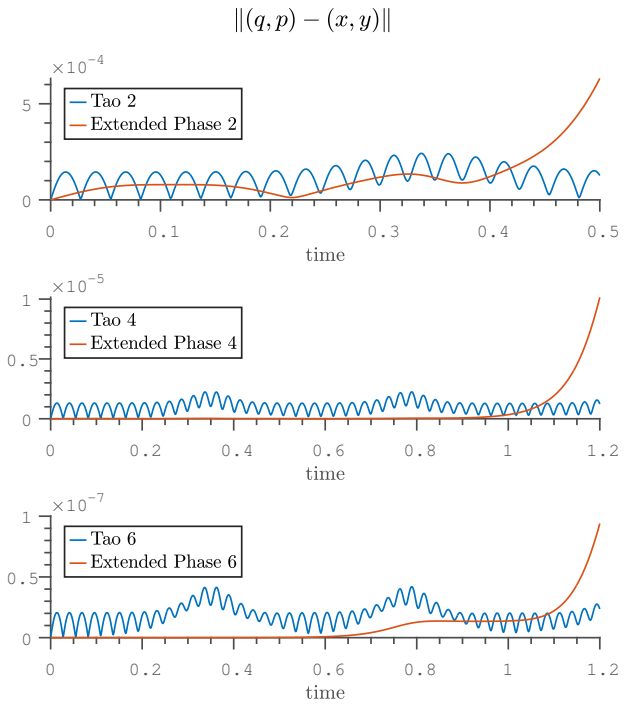

FIGURE 4. Defect $\|(q, p) - (x, y)\|$ in phase space copies with Pihajoki's original extended phase space integrator (6) and Tao's modified method (8) when solving NLS with $N = 5$. Note that the defect for our semiexplicit method (not plotted) would be the same order as the tolerance ϵ (10^{-10} or 10^{-13}) used in the symmetric projection step, and are negligibly small compared to theirs.

However, this defect $(x - q, y - p)$, albeit small, seems to affect the accuracy of preserving invariants. In order to demonstrate it, we solved the above NLS system using our semiexplicit method to compare the results with those of Tao's method. We chose the time step as $\Delta t = 10^{-3}$ because this system exhibits weak turbulence (see Dyachenko et al. [8]), and also used a relaxed tolerance of $\epsilon = 10^{-10}$ for the simplified Newton iterations (24) for faster computations.

Figure 5 shows the time evolution of two invariants of the system—Hamiltonian and total mass I—for the semiexplicit method and Tao's method both with the Triple Jump composition technique. While both methods preserve the invariants well without drifts, one clearly sees that our method has a much better accuracy. In fact, the results seem to indicate that Tao's method picks up errors in the invariants roughly proportional to the defect $(x - q, y - p)$; compare with Figure 4.

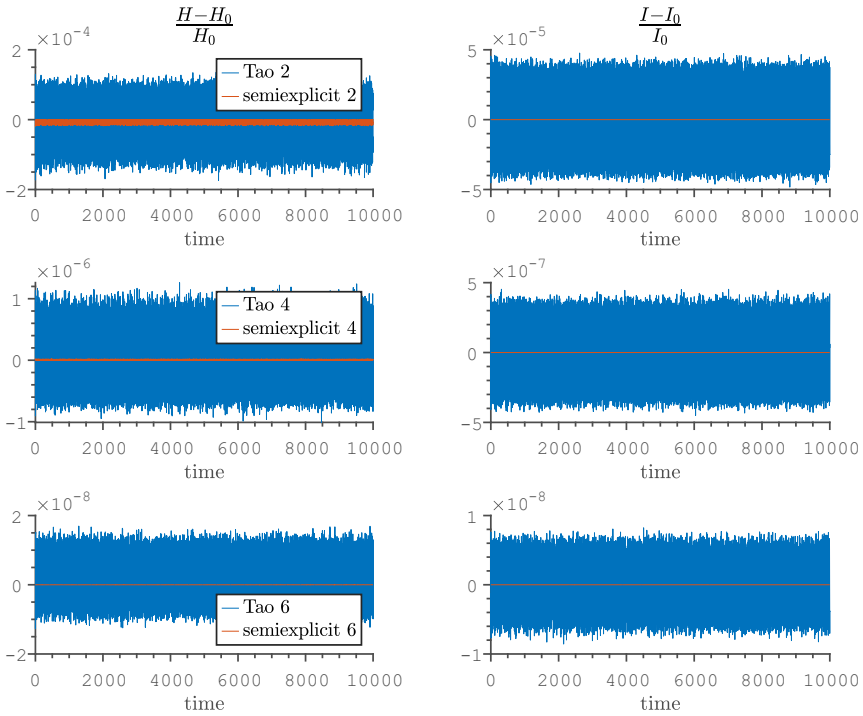

FIGURE 5. Comparison of preservation of two invariants (H and I; see (28) and (29)) between Tao's method ($\omega = 100$) and proposed semiexplicit method ($\epsilon = 10^{-10}$) for NLS system with $N = 5$ and time step $\Delta t = 10^{-3}$. higher-order methods for both methods are constructed using Triple Jump technique (21). The subscript $(\,\cdot\,)_0$ signifies the initial value.

For a further demonstration, Figure 6 shows a comparison of our method with the 2nd- and 4th-order Gauss–Legendre methods, for the same NLS problem as above but using a smaller tolerance of $\epsilon = 10^{-13}$ for both the semiexplicit and implicit methods. We also used Suzuki's and Yoshida's methods for higher-order methods in addition to the Triple Jump method.

Notice that, for the Implicit Midpoint (or the 2nd-order Gauss–Legendre) method, one observes a drift in the total mass. Since the Gauss–Legendre methods preserve quadratic invariants exactly (see Cooper [6] and Hairer et al. [11, Theorems IV.2.1 and IV.2.2]), the culprit for the drift would be the accumulated error from the nonlinear solver (Newton's method here); the tolerance here is $\epsilon = 10^{-13}$. Notice that our method exhibits no such drift, despite using the same tolerance with a simplified Newton method.

We also observe that Suzuki's composition has a better accuracy than the Triple Jump, especially in preserving the Hamiltonian for the 4th-order methods, and also that Yoshida's 6th-order method performs as well as Suzuki's, despite having much fewer stages and hence much faster as we shall see below.

As the third demonstration using another example, consider the motion of N point vortices in $\mathbb{R}^2$ with circulations $\{\Gamma_i \in \mathbb{R}\backslash\{0\}\}_{i=1}^N$ (see, e.g., Newton [18,

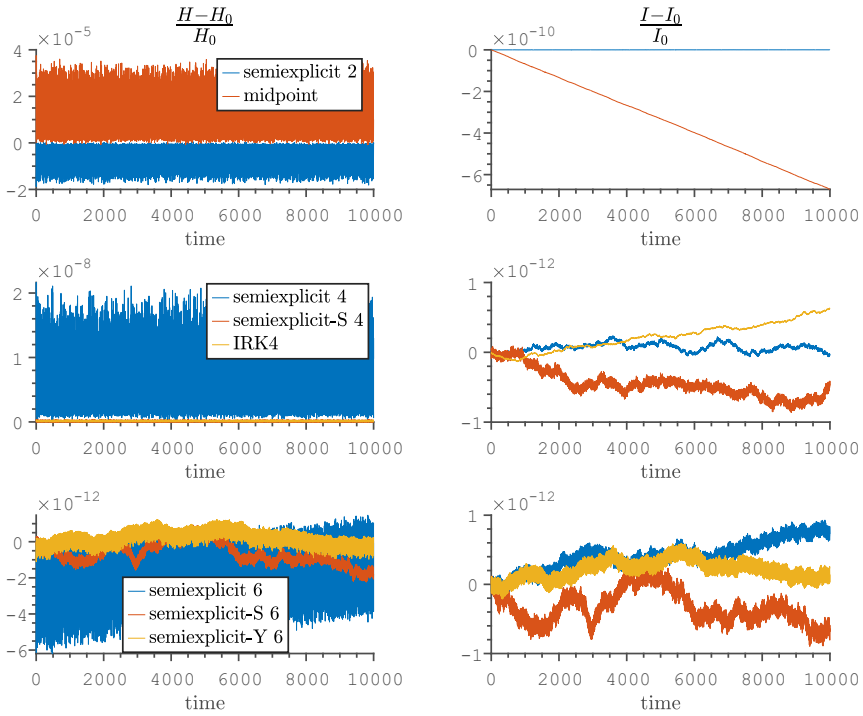

FIGURE 6. Comparison of same invariants from Figure 5 with more strict tolerance of $\epsilon = 10^{-13}$, time step $\Delta t = 10^{-3}$ and different methods: Higher-order semiexplicit methods with Triple Jump and Suzuki's and Yoshida's compositions (with labels "S" and "Y" respectively), as well as the 2^{nd}- and 4^{th}-order Gauss–Legendre methods (referred to as midpoint and IRK).

Section 2.1] and Chorin and Marsden [4, Section 2.1]). Interactions of them make their centers $\{z_i := (x_i, y_i) \in \mathbb{R}^2\}_{i=1}^N$ move according to the equations

$$\dot{x}_j = -\frac{1}{2\pi} \sum_{\substack{1 \le i \le N \\ i \ne j}} \frac{\Gamma_i (y_j - y_i)}{\|z_i - z_j\|^2}, \qquad \dot{y}_j = \frac{1}{2\pi} \sum_{\substack{1 \le i \le N \\ i \ne j}} \frac{\Gamma_i (x_j - x_i)}{\|z_i - z_j\|^2}.$$

Taking the interaction energy of the vortex system given by

$$H(x, y) := -\frac{1}{4\pi} \sum_{i \ne j} \Gamma_i \Gamma_j \log \|z_i - z_j\| \tag{30}$$

as the Hamiltonian, this system can be represented as a canonical Hamiltonian system (1) with $d = N$ by a simple coordinate transformation:

$$q_i := \sqrt{|\Gamma_i|}\, x_i, \qquad p_i := \sqrt{|\Gamma_i|}\, \operatorname{sgn}(\Gamma_i)\, y_i,$$

where $\operatorname{sgn}(x)$ is 1 if $x > 0$ and -1 otherwise. Note that the Hamiltonian is again non-separable. This system has three invariants in addition to the Hamiltonian:

$$Q := \sum_{i=1}^N \Gamma_i x_i, \qquad P := \sum_{i=1}^N \Gamma_i y_i. \qquad I := \sum_{i=1}^N \Gamma_i \|z_i\|^2, \tag{31}$$

where (Q, P) is called the linear impulse, and I is called the angular impulse.

Our test case has 10 vortices ($N = 10$) with the following initial condition and circulations:

$$
\begin{aligned}
x(0) &= (3, -10, 6, 9, 0, 7, -8, 5, 9, 7), \\
y(0) &= (-5, -6, 0, -2, 0, 10, 2, 9, 0, -1), \\
\Gamma &= \frac{1}{10}(-5, 3, 6, 7, -2, -8, -9, -3, 7, -6).
\end{aligned} \tag{32}
$$

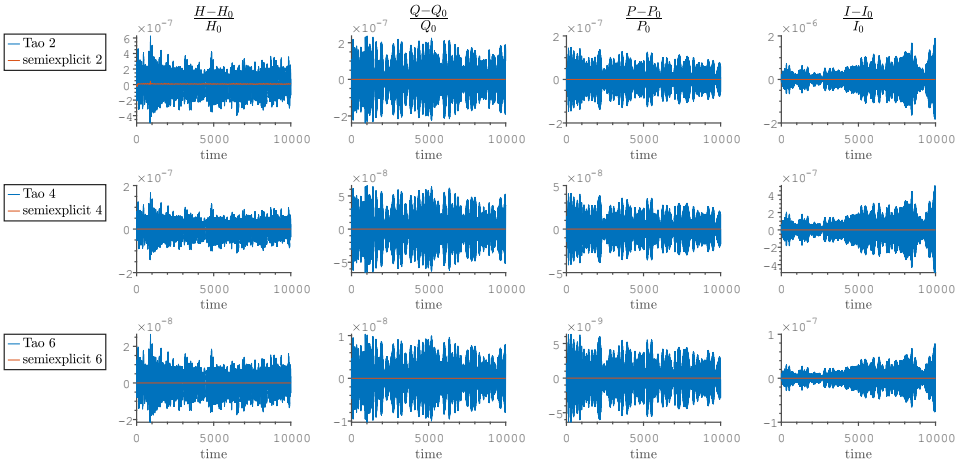

FIGURE 7. Comparison of preservation of four invariants (H, Q, P, and I; see (30) and (31)) between Tao's method ($\omega = 7$) and proposed semiexplicit method ($\epsilon = 10^{-10}$) for the 10-vortex system with time step $\Delta t = 0.1$. higher-order methods for both methods are constructed using Triple Jump technique (21). The subscript $(\,\cdot\,)_0$ signifies the initial value.

Figure 7 shows the results from solving this system using Tao's and our semiexplicit methods; the time step is $\Delta t = 0.1$ and the tolerance is $\epsilon = 10^{-10}$. Again we observe that our semiexplicit method outperforms Tao's method in preserving the four invariants.

Figure 8 shows further comparisons with other methods including the Gauss–Legendre methods with a more strict tolerance of $\epsilon = 10^{-13}$ for both the semiexplicit and implicit methods. We see that the proposed semiexplicit method is comparable to the Gauss–Legendre methods in preserving all the four invariants. Given that the Gauss–Legendre methods are known to preserve quadratic invariants exactly (see Cooper [6] and Hairer et al. [11, Theorems 2.1 and 2.2]), this result demonstrates that our method exhibits an excellent long-time behavior in preserving the invariants.

Also compare the errors of Tao's method in the invariants Q, P, and I from Figure 7 and those of ours from Figure 8. The errors are significantly smaller with our method, indicating that the defect $(x - q, y - p)$ (and possibly also the symplecticity in the original phase space) affects the errors in the invariants. This observation underscores the importance of our symmetric projection step.

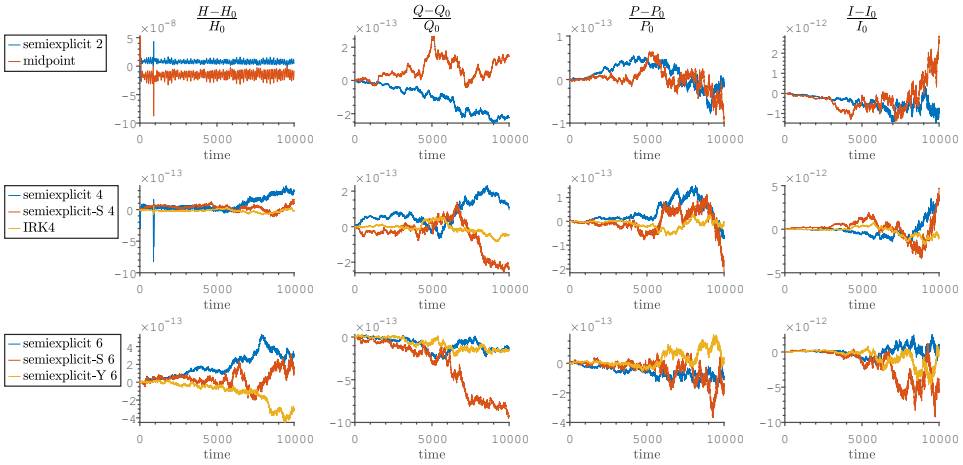

FIGURE 8. Comparison of same invariants from Figure 7 with more strict tolerance of $\epsilon = 10^{-13}$, time step $\Delta t = 0.1$ and various other methods: Higher-order semiexplicit methods with Triple Jump and Suzuki's and Yoshida's compositions (with labels "S" and "Y" respectively), as well as the 2^{nd}- and 4^{th}-order Gauss–Legendre methods (referred to as midpoint and IRK).

4.5. **Computational Efficiency.** Now that we have seen that our method exhibits desirable accuracies and long-time behaviors, a natural question to ask is whether it is as fast as Tao's explicit method, or at least faster than those implicit Gauss–Legendre methods. So we would like to compare the computation times of those methods discussed above when applied to the NLS and the vortex problems using the same initial values and time steps from above.

Table 1 compares the computation times and average number of iterations of various methods applied to the NLS problem; see the caption for details.

The columns labeled by `NW_itr` shows the average number of iterations required in the implicit part of each method. We see that our semiexplicit method requires fewer iterations than the Gauss–Legendre methods (Midpoint and IRK4). One may attribute the slowness of these implicit methods to full Newton's method used by them, but switching to quasi-Newton methods such as Broyden's method would not make these methods faster than ours because it is unlikely to curtail the disparity in the number of iterations. We note that the number of iterations is a good measure of how these methods compare because the implicit methods and our methods solve nonlinear equations for the same number of unknowns: $(q, p) \in \mathbb{R}^{2d}$ for the implicit methods and $\mu \in \mathbb{R}^{2d}$ for ours. Now, one may explain the disparity in the number of iterations as follows: Both use 0 as the initial guess, but the implicit methods need to solve for the $O(\Delta t)$ difference between (q_n, p_n) and (q_{n+1}, p_{n+1}), whereas ours needs to solve for μ, which is essentially the defect after a single step; one may estimate it to be proportional to the local error of the explicit integrator employed, i.e., $O((\Delta t)^{n+1})$ for an n-th order method, because the defect is a quantity that vanishes for the exact solution. This also explains why our method requires less iterations for higher-order methods.

TABLE 1. Comparison of computation times of various methods when solving NLS system with $N = 5$ from Section 4.4 with time step $\Delta t = 10^{-3}$ and terminal time $T = 1000$. Tao's method uses $\omega = 100$; its higher-order versions (Tao 4 and Tao 6) use the Triple Jump technique, and so does our standard semiexplicit method (semiexplicit 4 and semiexplicit 6). Those referred to as semiexplicit-S and semiexplicit-Y are our semiexplicit methods using Suzuki's and Yoshida's compositions, respectively. `Time` is the computation time in seconds averaged over 10 simulations, whereas `NW_itr` is the average number of Newton-type iterations used per step for both the simplified Newton (24) and Broyden's method (26). For the Midpoint and IRK4, the full Newton iteration is used. Computations were performed using MATLAB on a computer with Intel Core i7-8565U processor running at 1.80GHz.

$\epsilon = 10^{-10}$	Simplified (24)		Broyden (26)	
method	`Time`	`NW_itr`	`Time`	`NW_itr`
Tao 2	7.03		7.03	
semiexplicit 2	33.24	3.37	42.12	3.40
Midpoint	115.94	5.99	115.94	5.99
Tao 4	17.10		17.10	
semiexplicit 4	32.50	1.94	36.97	1.94
semiexplicit-S 4	26.95	1.09	26.96	1.09
IRK4	235.30	5.21	235.30	5.21
Tao 6	44.75		44.75	
semiexplicit 6	37.90	1.00	36.98	1.00
semiexplicit-S 6	90.19	1.00	88.83	1.00
semiexplicit-Y 6	31.65	1.00	30.68	1.00

$\epsilon = 10^{-13}$	Simplified (24)		Broyden (26)	
method	`Time`	`NW_itr`	`Time`	`NW_itr`
Tao 2	7.03		7.03	
semiexplicit 2	44.71	5	59.48	4.90
Midpoint	145.74	7.89	145.74	7.89
Tao 4	17.10		17.10	
semiexplicit 4	46.37	3	56.23	3
semiexplicit-S 4	50.13	2.28	55.34	2.29
IRK4	299.09	6.98	299.09	6.98
Tao 6	44.75		44.75	
semiexplicit 6	67.37	1.98	72.34	1.98
semiexplicit-S 6	86.30	1.00	84.04	1.00
semiexplicit-Y 6	31.46	1.02	29.37	1.02

Notice also that, although our 2^{nd}-order method is much slower than Tao's, it catches up with Tao's as the order of the method increases. Particularly our 6^{th}-method with a relaxed tolerance of $\epsilon = 10^{-10}$ is faster than Tao's of the same order. Moreover, recall from the last row of Figure 5 (plots from the same problem) shows that our 6^{th}-order method is much more accurate than Tao's. It is also notable

that the semiexplicit method with Yoshida's composition is much faster than Tao's 6^{th}-order method with Triple Jump thanks to the fewer steps involved in Yoshida's composition.

Table 2 shows the same comparison for the 10-vortex system. We show results only with the simplified Newton method (24) here for the reason stated in the caption. Note that the 10-vortex system is 20-dimensional whereas the NLS with $N = 5$ from above is 10-dimensional. We observe that our 4^{th}- and 6^{th}-order methods are faster than Tao's of the same orders even with $\epsilon = 10^{-13}$.

TABLE 2. Comparison of computation times of various methods when solving the 10-vortex system from Section 4.4 with time step $\Delta t = 0.1$ and terminal time $T = 1000$. We show results only with the simplified Newton method (24) because Broyden's method (26) gives more or less the same result. This is because the average number of iterations `NW_itr` is usually very close to 1 here: these two methods share exactly the same first iteration step and so there is almost no difference between them when `NW_itr` ≈ 1. The other details are the same as Table 1 except $\omega = 7$ for Tao's method.

	$\epsilon = 10^{-10}$		$\epsilon = 10^{-13}$	
method	`Time`	`NW_itr`	`Time`	`NW_itr`
Tao 2	1.82		1.82	
semiexplicit 2	3.00	2	4.29	3
Midpoint	18.17	4.18	22.77	5.42
Tao 4	5.32		5.32	
semiexplicit 4	4.10	1.00	4.25	1.05
semiexplicit-S 4	6.59	1	6.76	1.01
IRK4	45.99	4.01	57.05	4.99
Tao 6	15.63		15.63	
semiexplicit 6	11.92	1	12.03	1.00
semiexplicit-S 6	32.29	1	32.48	1.00
semiexplicit-Y 6	9.23	1	9.49	1.00

A possible explanation of why our method can be faster than Tao's for higher-order methods and higher-dimensional problems is the following: Recall that Tao's 2^{nd}-order method (8) is a composition of 5 flows, whereas our explicit part (6) is a composition of 3 flows. Therefore, for the 4^{th}-order method using the Triple Jump (21), Tao's involves 15 stages whereas ours involves 9 stages, and for the 6^{th}-order method, Tao's 45 stages whereas ours 27 stages. Now, notice in Tables 1 and 2 that the number of Newton-type iterations, `NW_itr`, gets smaller for higher-order methods and higher-dimensional problems, eventually becoming close to 1 in Table 2. This means that only one step of Newton-type iteration is performed in the projection step most of the time. In other words, in the simplified Newton iteration (24), $\mu^{(0)}$ or $\mu^{(1)}$ is usually taken as μ, but then since $\mu^{(0)} = 0$, we have, using (23) and (24),

$$\mu^{(1)} = -\frac{1}{4} A\, \hat{\Phi}_{\Delta t}(\zeta_n).$$

Note that $\hat{\Phi}_{\Delta t}(\zeta_n)$ is already computed in the explicit part of the method, and so computing $\mu^{(1)}$ does not involve extra stages of discrete time evolutions (which would

be required to compute $\mu^{(k)}$ *for* $k \geq 2$*).* Therefore, if `NW_itr` ≈ 1, the projection step becomes very simple and hence may require fewer computations compared to the extra stages in Tao's method.

Moreover, as the dimension of the problem increases, each stage becomes computationally more expensive, and so the computational advantage due to the difference in the number of stages would be amplified.

See Appendix A for a further numerical study of the projection step. The results from above and Appendix A suggest the following:

- The projection step requires very few iterations when the time step Δt is small enough compared to the scale of the problem.
- Increasing Δt may result in a significant increase in the number of iterations, and hence a slowdown of our method; see Table 3 in Appendix A.
- The simplified Newton method (24) occasionally fails to converge within a reasonable number of iterations, but works well in many cases. Hence the convergence issue is not detrimental in the long run; see Table 6 in Appendix A.
- Broyden's method (26) tends to reduce the number of required iterations slightly, and seems as fast as the simplified Newton method. It also resolves the convergence issue of the simplified Newton method mentioned above; see Table 6 in Appendix A.

In conclusion, using a small enough Δt seems to be the key to an efficient implementation of our semiexplicit method. Also, higher-order methods tend to require less iterations in the projection step. The reason seems to be that smaller Δt and higher-order methods produce smaller defects in the explicit time evolution, hence less iterations in the projection step to eliminate the defects produced.

Appendix A. Numerical Study of Projection Step

A.1. **Effect of Time Step and Parameters?** This appendix gives a further numerical study of the simplified Newton method (Section 4.1) and Broyden's method (Section 4.2) in the projection step. The purpose of this appendix is to numerically investigate the following questions: (i) How are these nonlinear solvers affected by a change in the time step as well as a change in the parameters of the problems? (ii) Does Broyden's method offer a significant improvement of the simplified Newton method?

A.2. **NLS Problem with Larger Time Step.** Let us first see how the time step affects the nonlinear solvers by changing Δt from 10^{-3} to 10^{-2} in the NLS problem.

Compare Table 3 ($\Delta t = 10^{-2}$) with Table 1 ($\Delta t = 10^{-3}$). We observe that the change in Δt results in significantly more numbers of iterations to achieve convergence in the projection step, and hence a significant slowdown of our integrator. It also shows that, even with the increased number of iterations, Broyden's method is as fast as the simplified Newton method. We also notice that Broyden's method tends to require less iterations.

Table 4 makes a further comparison of the average numbers of iterations for a longer time interval $0 \leq t \leq 10^4$ along with the maximum errors in the projection step and the resulting maximum defects. Again, Broyden's method requires less iterations in the long run too, as one might expect from the theory mentioned in Section 4.2.

TABLE 3. Comparison of computation times of various methods when solving the NLS system with $N = 5$ from Section 4.4 with time step $\Delta t = 10^{-2}$ and terminal time $T = 10^3$ using both the simplified Newton (24) and Broyden's method (26). The other details are the same as Table 1.

	$\epsilon = 10^{-10}$				$\epsilon = 10^{-13}$			
	Simplified (24)		Broyden (26)		Simplified (24)		Broyden (26)	
method	`Time`	`NW_itr`	`Time`	`NW_itr`	`Time`	`NW_itr`	`Time`	`NW_itr`
Tao 2	0.76		0.76		0.76		0.76	
semiex 2	7.72	8.54	8.71	6.90	10.27	11.55	11.04	8.88
Midpoint	25.77	12.87	25.77	12.87	33.60	16.66	33.60	16.66
Tao 4	1.85		1.85		1.85		1.85	
semiex 4	10.72	6.79	11.47	5.78	15.11	9.88	15.13	7.85
semiex-S 4	12.53	5.50	13.07	4.98	18.95	8.56	18.46	6.95
IRK4	48.60	10.65	48.60	10.65	60.50	13.49	60.50	13.49
Tao 6	4.82		4.82		4.82		4.82	
semiex 6	20.91	5.93	19.44	5.00	31.02	8.92	28.24	7.06
semiex-S 6	15.69	1.78	16.49	1.78	41.12	4.69	39.84	4.30
semiex-Y 6	11.30	3.91	13.39	3.93	19.88	6.91	19.29	5.99

TABLE 4. Comparison of convergence and errors of various methods when solving the NLS system with $N = 5$ from Section 4.4 with time step $\Delta t = 0.01$ and terminal time $T = 10^4$ using both the simplified Newton (24) and Broyden's method (26). `Max_Error` denotes the maximum of $\left\|\mu^{(N+1)} - \mu^{(N)}\right\|$ (see (25)) among all projection steps (hence is approximately ϵ) whereas `Max_Defect` denotes the maximum of defects $\|(q,p) - (x,y)\|$ in each solution. The other details are the same as Table 1.

	$\epsilon = 10^{-13}$					
	Simplified (24)			Broyden (26)		
method	`NW_itr`	`Max_Error`	`Max_Defect`	`NW_itr`	`Max_Error`	`Max_Defect`
Tao 2			0.025191			0.025191
semiex 2	11.55	1e-13	4e-13	8.88	1e-13	4.39e-13
Midpoint	16.66	1e-13		16.66	1e-13	
Tao 4			0.016279			0.016279
semiex 4	9.87	1e-13	4e-13	7.85	9.99e-14	4.21e-13
semiex-S 4	8.56	1e-13	4e-13	6.95	1e-13	4.39e-13
IRK4	13.50	1e-13		13.50	1e-13	
Tao 6			0.006048			0.006048
semiex 6	8.93	9.99e-14	4e-13	7.06	1e-13	4.28e-13
semiex-S 6	4.69	1e-13	4e-13	4.31	1e-13	4.22e-13
semiex-Y 6	6.91	1e-13	4e-13	5.99	9.99e-14	4.17e-13

Notice in the `Max_Defect` columns that the projection step suppresses the phase space defect $\|(q,p) - (x,y)\|$ to the order of the tolerance $\epsilon = 10^{-13}$—significantly smaller than Tao's. These defects seem to affect the errors of the solutions: Figures 9 and 10 show the time evolution of two invariants (using Broyden's method) of the system with $\Delta t = 10^{-2}$ just as we did in Figures 5 and 6, respectively with $\Delta t = 10^{-3}$. What is particularly notable is that, as Δt increases, the error in the total mass I increased significantly for Tao's whereas it stays very small for ours.

Therefore, our method, although our method is now much slower than Tao's, still gives much more accurate results than Tao's.

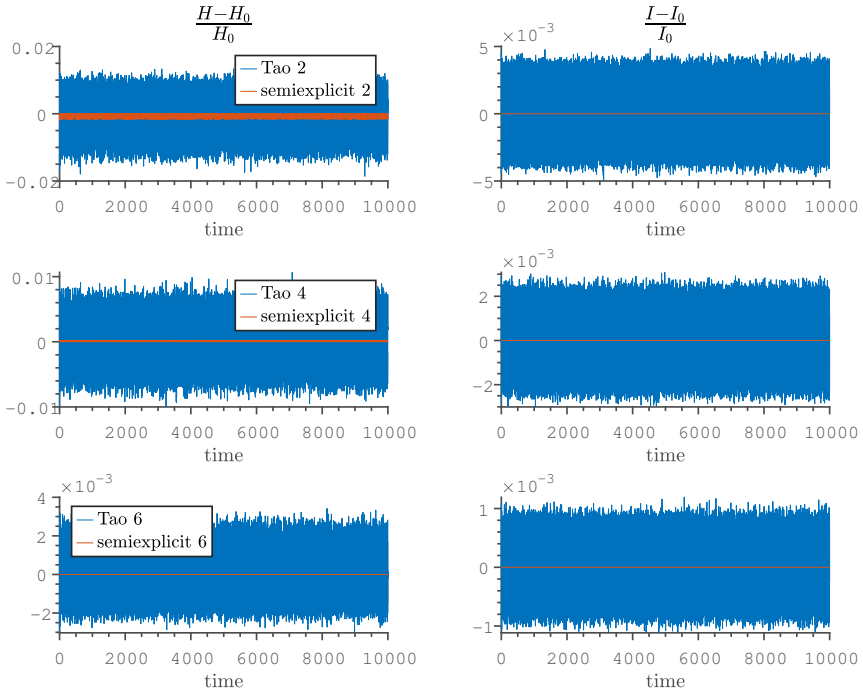

FIGURE 9. Same plots as Figure 5 except with a larger time step $\Delta t = 10^{-2}$ instead of $\Delta t = 10^{-3}$.

A.3. **10-Vortex Problem with Disparate Circulations.** Let us modify the 10-vortex problem with the following initial conditions and circulations to create a problem that requires more Newton-type iterations in the projection step.

$$\begin{aligned} x(0) &= (0.5, 3.5, -1.5, -0.5, -4.5, -3.5, 1.5, -2, 4, -4), \\ y(0) &= (5, 0.5, 2, 5, -2, -1, -0.5, 3, 3.5, -4), \\ \Gamma &= (-14.8, -18.8, 17.6, -8, -8.2, -6.8, -1.4, 6, -11, 13.8). \end{aligned} \tag{33}$$

Compare this to the previous parameters (32) where $-1 < \Gamma_i < 1$ for $i = 1, \ldots, 10$. The circulations now have more disparities among the vortices. This means that vortices move in different time scales, making the problem more challenging in selecting the time step. Accordingly, we have chosen a smaller time step $\Delta t = 0.01$ here.

Table 5 shows the average computation times as well as the average number of iterations for this problem just as in Table 2 for $0 \le t \le 100$. We observe an increase in the average number of iterations and hence a slight slowdown of our method. As a result, our method is slightly slower than Tao's with $\epsilon = 10^{-13}$, although with $\epsilon = 10^{-10}$, the our 6^{th}-order method is still faster than Tao's.

Table 6 shows the average numbers of iterations along with the maximum errors in the projection step and the resulting maximum defects computed for the longer

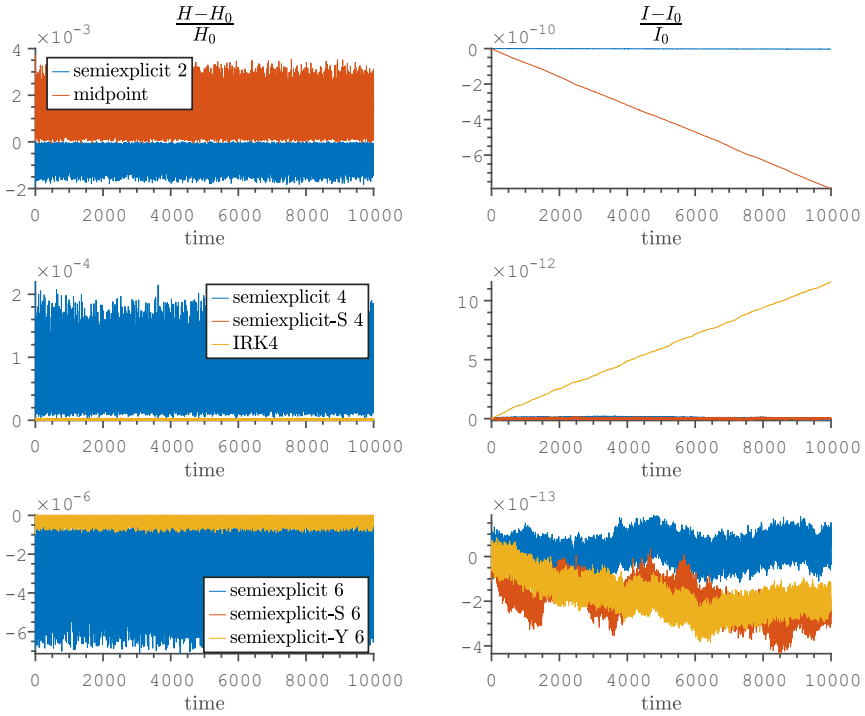

FIGURE 10. Same plots as Figure 6 except with a larger time step $\Delta t = 10^{-2}$ instead of $\Delta t = 10^{-3}$.

TABLE 5. Comparison of computation times of various methods when solving the 10-vortex system with parameters (33) in place of (32) and time step $\Delta t = 0.01$ and terminal time $T = 100$ using both the simplified Newton (24) and Broyden's method (26). The other details are the same as Table 2.

	$\epsilon = 10^{-10}$				$\epsilon = 10^{-13}$			
	Simplified (24)		Broyden (26)		Simplified (24)		Broyden (26)	
method	`Time`	`NW_itr`	`Time`	`NW_itr`	`Time`	`NW_itr`	`Time`	`NW_itr`
Tao 2	2.05		2.05		2.05		2.05	
semiex 2	5.04	3	5.01	3	8.12	5	7.68	4.55
Midpoint	24.50	4.62	24.50	4.62	31.12	5.77	31.12	5.77
Tao 4	5.96		5.96		5.96		5.96	
semiex 4	8.44	1.85	8.89	1.85	13.96	3	14.05	3
semiex-S 4	8.08	1.08	8.43	1.08	17.19	2.29	17.86	2.28
IRK4	58.71	4.30	58.71	4.30	73.88	5.25	73.88	5.25
Tao 6	17.67		17.67		17.67		17.67	
semiex 6	13.35	1.00	13.61	1.00	24.36	1.80	25.28	1.80
semiex-S 6	37.15	1.00	37.15	1.00	40.60	1.08	40.58	1.08
semiex-Y 6	10.51	1	10.42	1	11.01	1.03	11.09	1.03

TABLE 6. Comparison of convergence and errors of various methods when solving the challenging 10-vortex system with time step $\Delta t = 0.01$ and a longer terminal time $T = 1000$ using both the simplified Newton (24) and Broyden's method (26). `Max_Err` denotes the maximum of $\left\|\mu^{(N+1)} - \mu^{(N)}\right\|$ (see (25)) among all projection steps (hence is approximately ϵ) whereas `Max_Def` denotes the maximum of defects $\|(q,p) - (x,y)\|$ in each solution. The star * indicates that the Newton iteration was stopped at $N = 100$ before it converged, hence resulting in `Max_Err` larger than ϵ. The other details are the same as Table 2.

	$\epsilon = 10^{-13}$					
	Simplified (24)			Broyden (26)		
method	`NW_itr`	`Max_Err`	`Max_Def`	`NW_itr`	`Max_Err`	`Max_Def`
Tao 2			0.00376			0.00376
semiex 2	5.27*	1.67e-13	6.66e-13	4.46	9.99e-14	6.57e-13
Midpoint	5.71	9.99e-14		5.71	9.99e-14	
Tao 4			8.38e-06			8.38e-06
semiex 4	3.59*	1.62e-13	6.47e-13	3.05	9.99e-14	7.32e-13
semiex-S 4	2.64*	1.61e-13	6.44e-13	2.45	1e-13	7.11e-13
IRK4	5.58*	1.18e-13		5.58*	1.18e-13	
Tao 6			2.09e-07			2.09e-07
semiex 6	1.97*	1.42e-13	5.69e-13	1.90	9.99e-14	7.15e-13
semiex-S 6	1.40*	1.16e-13	4.62e-13	1.41	9.99e-14	7.84e-13
semiex-Y 6	1.14	1e-13	4e-13	1.14	9.99e-14	5.41e-13

interval $0 \le t \le 1000$. Overall, there is a slight increase in the average number of iterations for every method. Particularly, notice those numbers marked with star * in the `NW_itr` first column. These are the instances where the simplified Newton method did not converge to the desired value μ with $\epsilon = 10^{-13}$ within 100 steps at some point in the simulation. However, the only slight increases in `NW_itr` compared to those in Table 5 suggest that these are rather rare instances. Notice also that this issue of convergence is resolved by using Broyden's method.

Figures 11 and 12 show the time evolution of the invariants (using Broyden's method) just as we did in Figures 7 and 8 with different parameters. Notice that, although Tao's method is faster in most cases, its errors in some invariants increased whereas ours either stayed in the same level or became smaller. It is also worth mentioning that, the last row of Figure 11 is the instance where our method is faster than Tao's, and ours is much more accurate than Tao's.

A.4. **Conclusion of Numerical Study.** The above numerical experiments suggest first that the time step and the parameters of the problem affect the number of iterations in the projection step considerably. Particularly, the NLS example in Appendix A.2 shows that increasing the time step may result in a significant increase in the number of iterations. The 10-vortex example in Appendix A.3 shows that the change in the parameters also affects the convergence of the projection step too, but can be compensated by selecting an appropriate time step Δt, again underscoring the importance of selecting a small enough Δt.

The results also show that Broyden's method is as fast as the simplified Newton method, and is more robust in the sense that it does not experience the convergence issue that the simplified Newton method occasionally did. However, the

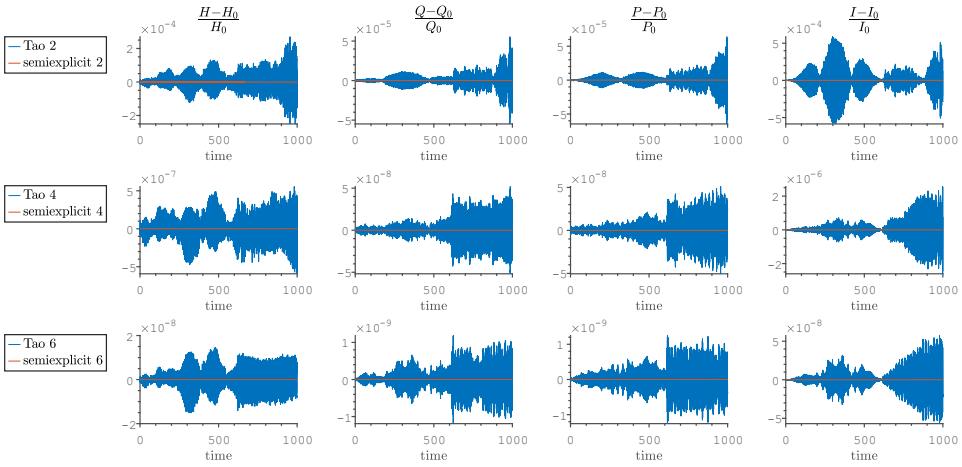

FIGURE 11. Same plots as Figure 7 except with parameters (33) and $\Delta t = 0.01$ instead of (32) and $\Delta t = 0.1$.

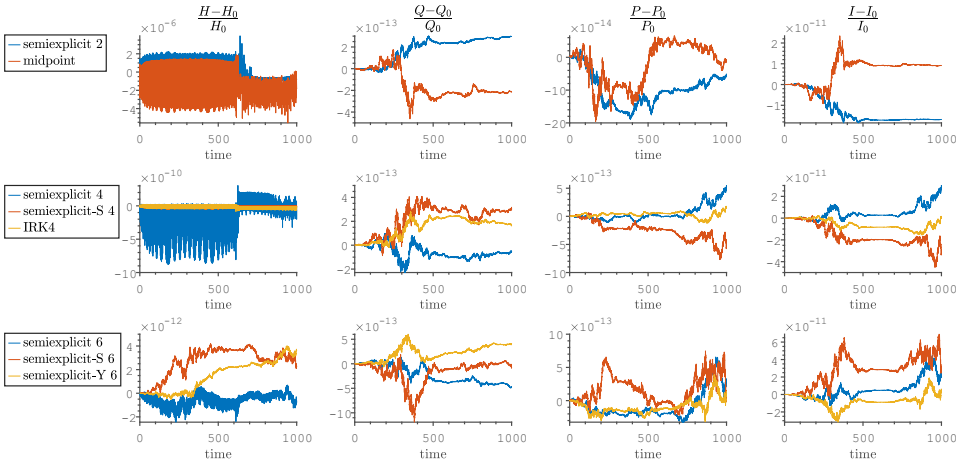

FIGURE 12. Same plots as Figure 8 except with parameters (33) and $\Delta t = 0.01$ instead of (32) and $\Delta t = 0.1$.

convergence issue is rather minor, and the overall difference between the two methods is fairly small, suggesting that the simplified Newton method is quite effective despite its simplicity.

ACKNOWLEDGMENTS

We would like to thank Molei Tao for helpful discussions, and Joshua Burby, Michael Kraus, and Xin Wu for insightful comments. We also would like to thank the reviewer for the questions and comments that helped us improve the paper. This work was supported by NSF grant DMS-2006736.

Note added in Proof. The numerical results suggest that our semiexplicit integrator preserves both the total mass I (see (29) of the NLS problem and the

angular impulse I (see (31)) of the vortex problem—both quadratic invariants. In fact, our semiexplicit integrator preserves any quadratic invariant of the original Hamiltonian system (1). We shall report on this in the forthcoming paper [19].

References

[1] S. Blanes. Symplectic maps for approximating polynomial Hamiltonian systems. *Physical Review E*, 65(5):056703, 2002.

[2] C. G. Broyden. A class of methods for solving nonlinear simultaneous equations. *Mathematics of computation*, 19(92):577–593, 1965.

[3] S. A. Chin. Explicit symplectic integrators for solving nonseparable Hamiltonians. *Physical Review E*, 80(3):037701, 2009.

[4] A. J. Chorin and J. E. Marsden. *A Mathematical Introduction to Fluid Mechanics*, volume 4 of *Texts in Applied Mathematics*. Springer, 1993.

[5] J. Colliander, M. Keel, G. Staffilani, H. Takaoka, and T. Tao. Transfer of energy to high frequencies in the cubic defocusing nonlinear Schrödinger equation. *Inventiones Mathematicae*, 181(1):39–113, 2010.

[6] G. J. Cooper. Stability of Runge-Kutta methods for trajectory problems. *IMA Journal of Numerical Analysis*, 7(1):1–13, 1987.

[7] M. Creutz and A. Gocksch. Higher-order hybrid Monte Carlo algorithms. *Phys. Rev. Lett.*, 63:9–12, 1989.

[8] S. Dyachenko, A. Newell, A. Pushkarev, and V. Zakharov. Optical turbulence: weak turbulence, condensates and collapsing filaments in the nonlinear schrödinger equation. *Physica D: Nonlinear Phenomena*, 57(1):96–160, 1992.

[9] E. Forest. Canonical integrators as tracking codes (or how to integrate perturbation theory with tracking). *AIP Conference Proceedings*, 184(1):1106–1136, 1989.

[10] D. M. Gay. Some convergence properties of Broyden's method. *SIAM Journal on Numerical Analysis*, 16(4):623–630, 1979.

[11] E. Hairer, C. Lubich, and G. Wanner. *Geometric Numerical Integration: Structure-Preserving Algorithms for Ordinary Differential Equations*. Springer, Berlin, Heidelberg, 2nd edition, 2006.

[12] B. Leimkuhler and S. Reich. *Simulating Hamiltonian dynamics*, volume 14 of *Cambridge Monographs on Applied and Computational Mathematics*. Cambridge University Press, Cambridge, 2004.

[13] D. Li and X. Wu. Modification of logarithmic Hamiltonians and application of explicit symplectic-like integrators. *Monthly Notices of the Royal Astronomical Society*, 469(3):3031–3041, 2017.

[14] L. Liu, X. Wu, G. Huang, and F. Liu. Higher order explicit symmetric integrators for inseparable forms of coordinates and momenta. *Monthly Notices of the Royal Astronomical Society*, 459(2):1968–1976, 2016.

[15] J. Luo, X. Wu, G. Huang, and F. Liu. Explicit symplectic-like integrators with midpoint permutations for spinning compact binaries. *The Astrophysical Journal*, 834(1):64, 2017.

[16] F. Mannel. On the order of convergence of Broyden's method. *Calcolo*, 58(4): 1–21, 2021.

[17] R. I. McLachlan and G. R. W. Quispel. Explicit geometric integration of polynomial vector fields. *BIT Numerical Mathematics*, 44(3):515–538, 2004.

[18] P. K. Newton. *The N-vortex problem*. Springer, New York, 2001.

[19] T. Ohsawa. Preservation of quadratic invariants by semiexplicit symplectic integrators for non-separable Hamiltonian systems. in progress.
[20] G. Pan, X. Wu, and E. Liang. Extended phase-space symplectic-like integrators for coherent post-Newtonian Euler-Lagrange equations. *Phys. Rev. D*, 104: 044055, 2021.
[21] P. Pihajoki. Explicit methods in extended phase space for inseparable Hamiltonian problems. *Celestial Mechanics and Dynamical Astronomy*, 121(3):211–231, 2015.
[22] J. Sanz-Serna and M. Calvo. *Numerical Hamiltonian Problems*. Dover Books on Mathematics. Dover Publications, 2018.
[23] G. Strang. On the construction and comparison of difference schemes. *SIAM Journal on Numerical Analysis*, 5(3):506–517, 1968.
[24] J. B. Sturgeon and B. B. Laird. Symplectic algorithm for constant-pressure molecular dynamics using a Nosé–Poincaré thermostat. *The Journal of Chemical Physics*, 112(8):3474–3482, 2000.
[25] M. Suzuki. Fractal decomposition of exponential operators with applications to many-body theories and monte carlo simulations. *Physics Letters A*, 146 (6):319–323, 1990.
[26] M. Tao. Explicit high-order symplectic integrators for charged particles in general electromagnetic fields. *Journal of Computational Physics*, 327:245–251, 2016.
[27] M. Tao. Explicit symplectic approximation of nonseparable Hamiltonians: Algorithm and long time performance. *Physical Review E*, 94(4):043303, 2016.
[28] Y. Wang, W. Sun, F. Liu, and X. Wu. Construction of explicit symplectic integrators in general relativity. I. Schwarzschild black holes. *The Astrophysical Journal*, 907(2):66, 2021.
[29] Y. Wang, W. Sun, F. Liu, and X. Wu. Construction of explicit symplectic integrators in general relativity. II. Reissner–Nordström black holes. *The Astrophysical Journal*, 909(1):22, 2021.
[30] Y. Wang, W. Sun, F. Liu, and X. Wu. Construction of explicit symplectic integrators in general relativity. III. Reissner–Nordström-(anti)-de Sitter black holes. *The Astrophysical Journal Supplement Series*, 254(1):8, 2021.
[31] X. Wu, Y. Wang, W. Sun, and F. Liu. Construction of explicit symplectic integrators in general relativity. IV. Kerr black holes. *The Astrophysical Journal*, 914(1):63, 2021.
[32] Y. K. Wu, E. Forest, and D. S. Robin. Explicit symplectic integrator for s-dependent static magnetic field. *Physical Review E*, 68(4):046502–, 2003.
[33] H. Yoshida. Construction of higher order symplectic integrators. *Physics Letters A*, 150(5):262–268, 1990.
[34] N. Zhou, H. Zhang, W. Liu, and X. Wu. A note on the construction of explicit symplectic integrators for Schwarzschild spacetimes. *The Astrophysical Journal*, 927(2):160, 2022.

Department of Mathematical Sciences, The University of Texas at Dallas, 800 W Campbell Rd, Richardson, TX 75080-3021
Email address: Buddhika.Jayawardana@utdallas.edu,tomoki@utdallas.edu